SOLAR WIND - MAGNETOSPHERE INTERACTION AS DETERMINED BY OBSERVATIONS AND A GLOBAL MHD SIMULATION

Minna Palmroth

12th May 2003

Preface

The work presented in this thesis has been carried out at the Department of Geophysical Research (GEO) of the Finnish Meteorological Institute (FMI). I am first and foremost indebted to my advisors Prof. Tuija Pulkkinen and Dr. Pekka Janhunen. Tuija's efficiency, her prompt pinpointing of relevant issues, and her wide knowledge of significant work in the field have greatly impressed me. Pekka's profound understanding of physics, in particular the MHD theory, has been crystallized in the form of GUMICS-4, the global MHD simulation that I have been privileged to use in my work. Pekka is also an excellent teacher: he rarely takes anything as self-evident and always seems to have time and patience to explain matters in detail. I feel lucky to have been granted a possibility to work with such front-line scientists.

I warmly thank Prof. Hannu Koskinen of the University of Helsinki for his continuous support and the excellent courses he teaches at the University. Despite of his tight schedule, Hannu always found time to discuss with me, carefully read through my various manuscripts, and provided relevant criticism on my work.

I wish to thank Professors Erkki Jatila and Petteri Taalas, the former and present Director General of the Finnish Meteorological Institute, and Prof. Risto Pellinen, the head of FMI/GEO, for providing me with the opportunity to work in such an innovative organization. I am immensely grateful to Dr. Risto Pirjola, the head of Space Physics group at GEO; it is probably impossible to find a boss who is as flexible and pleasant as Risto. I am sincerely grateful to Dr. Harri Laakso (ESTEC, the Netherlands), who first recruited me as a trainee at GEO, and who was also my first advisor during his time in Finland.

A number of people from GEO deserve to be acknowledged. Lasse Häkkinen, Dr. Johan Silén, Pasi Soljala and Petri Makkonen for finding the time to help me with computers. Special thanks go to Prof. Gilbert Leppelmeier for helping me with English. I warmly thank the people of the original "Nuorisodisco", consisting of Noora Partamies, Antti Pulkkinen, and Tuukka Säles, for a unique atmosphere of a shared office. In particular, I would like to thank the past and present members of the Geodynamo, one of the rare rock bands in the world with a PhD playing base, and the only one in which I have been singing. The staff of GEO is acknowledged for enriching my working days, the following people in particular: Maria Genzer (who also helped me to write understandable Finnish), Dr. Petri Toivanen, Jouni Polkko, Harri Auvinen, Dr. Kirsti Kauristie, Sanna Mäkinen, and Markku Mäkelä.

Several coworkers and co-authors are warmly acknowledged. I would like to thank Emilia Huttunen of the University of Helsinki; she is also a founding member of the united GEO/University soccer team, in which I enjoy playing. I am further grateful to Dr. Niescja Turner (University of Texas at El Paso), Dr. Eija Tanskanen (NASA Goddard Space Flight Center), W. K. Peterson (University of Colorado at Boulder), and C.-C. Wu (NASA Goddard Space Flight Center).

I wish to express my sincere gratitude to Professors Kalevi Mursula (University of Oulu) and Victor Sergeev (University of St. Petersburg) for their interest in this thesis and careful review of the manuscript.

This thesis is financially supported by the Academy of Finland. Furthermore, I wish to thank the Vilho, Yrjö and Kalle Väisälä Foundation, the Magnus Ehrnrooth Foundation, the Emil Aaltonen Foundation, and the Sohlberg Delegation for providing me with travel grants, which have helped me to get involved with the international space science community.

I would also like to thank my family and in-laws for their support and existence, and my friends for the same reason. Finally, I wish to express my deepest gratitude to my husband Kalle, whose effort pertaining this thesis was not only to support and encourage me: He also provided excellent ground-level comments on this thesis.

Helsinki, May 2003

Minna Palmroth

Summary of the thesis

Paper I: Palmroth, M., Laakso, H., and Pulkkinen, T. I., Location of high-altitude cusp during steady solar wind conditions, *J. Geophys. Res., 106*, 21,109-21,122, 2001.

Paper II: Huttunen, K. E. J., Koskinen, H. E. J., Pulkkinen, T. I., Pulkkinen, A., Palmroth, M., Reeves, E. G. D., and Singer, H. J., April 2000 magnetic storm: Solar wind driver and magnetospheric response, *J. Geophys. Res., 107*, doi:10.1029/2001JA009154, 2002.

Paper III: Palmroth, M., Janhunen, P, Pulkkinen, T. I., and Peterson, W. K., Cusp and magnetopause locations in global MHD simulation, *J. Geophys. Res., 106*, 29,435-29,450, 2001.

Paper IV: Palmroth, M., Pulkkinen, T. I., Janhunen, P., and Wu, C.-C., Stormtime energy transfer in global MHD simulation, *J. Geophys. Res., 108*, doi:10.1029/2002JA009446, 2003.

Paper V: Palmroth, M., Janhunen, P., Pulkkinen, T. I., and Koskinen, H. E. J., Ionospheric energy input as a function of solar wind parameters: global MHD simulation results, submitted to *Annales Geophysicae*, 2003.

All the data used in this thesis are calibrated data products provided by the corresponding instrument PI groups and distributed partly by the CDAWeb interface. The global MHD simulation and the corresponding visualization programs used in this thesis are written and designed by Pekka Janhunen. Routines for simulation data processing were developed by the author.

Paper I investigates the high-altitude cusp location statistically using Polar spacecraft measurements. In particular, the paper focuses on stationary cusp as the data set contains only events that occurred during steady solar wind conditions. Paper I is used to demonstrate the solar wind control on the shape of the magnetosphere with an easily distinguished observable: the cusp location. The author identified the events in the data base and carried out the statistical analysis.

Paper II investigates the chain of events that led to a large magnetic storm on 6 April 2000. The description of the solar and interplanetary space observations is followed by a detailed study of the magnetospheric response, together with an examination of ground effects of the storm as manifested by the observations of the geomagnetically induced currents. Paper II demonstrates the energy coupling of the solar wind and the magnetosphere as manifested by the global magnetospheric dynamics set up by the interplanetary conditions. The author's role was to participate in the analysis of the magnetospheric dynamics and solar wind-magnetosphere interaction.

Paper III investigates the effect of the interplanetary magnetic field and solar wind dynamic pressure on the cusp and subsolar magnetopause location in a global MHD simulation GUMICS-4. Paper III also compares the cusp location in the simulation to the observational cusp location of Paper I. Paper III both illustrates the solar wind

control on the shape of the magnetosphere as well as verifies the code performance. The simulation runs and the analysis of the results were carried out by the author.

Paper IV uses the GUMICS-4 MHD simulation to estimate quantitatively the energy input to the magnetosphere during the major storm of April 2000. Furthermore, Paper IV identifies the locations on the magnetopause surface, where significant energy transfer takes place in the MHD simulation. The author carried out the simulation runs and the analysis of the results.

Paper V investigates the ionospheric dissipation in the GUMICS-4 MHD simulation by calculating the amount of energy consumed by the Joule heating and electron precipitation. The results are compared with empirical proxies of the two parameters. The ionospheric energy calculation is carried out both for the 6 April 2000 storm simulation and to a simulation of a magnetospheric substorm on 15 August 2001. Paper V investigates further the latitudinal and longitudinal distribution of the energy dissipation during the two events. Finally, Paper V finds a high-correlation power law between the total ionospheric energy and solar wind parameters. Paper V also obtains theoretical scaling laws between the solar wind parameters and ionospheric dissipation. With the exception of the theoretical scaling laws developed by P. Janhunen, the main part of the work was carried out by the author.

A CD-rom Appendix is attached to this thesis. The Appendix CD contains animations of the global MHD simulation results; there are also some references to these animations in this thesis.

The global MHD simulation used in this thesis is defined in the Geocentric Solar Ecliptic (GSE) coordinate system, in which the X-axis points to the Sun, the Z axis is perpendicular to the ecliptic plane and is due north, and the Y axis completes the right-handed system, pointing duskward. The GSE coordinates are used throughout in this thesis.

Contents

1 Introduction 10
1.1 Structure of the magnetosphere 10
1.2 Energy transfer mechanisms 12
1.2.1 Magnetic reconnection 12
1.2.2 Other energy transfer mechanisms 17
1.3 Practical significance 18
1.3.1 Scope of this thesis 19

2 Manifestations of energy transfer: Magnetospheric dynamics 20
2.1 Cusp dynamics 20
2.2 Magnetospheric substorms 23
2.3 Magnetic storms 25

3 Global MHD simulations 28
3.1 The MHD description 28
3.2 Numerical solutions of MHD description 30
3.2.1 GUMICS-4 MHD simulation 33
3.2.2 GUMICS-4 relative to other global MHD simulations 35
3.3 Cusp and magnetopause in MHD 38
3.3.1 Code verification 39
3.3.2 Results: Cusp and subsolar magnetopause location in MHD . . . 39

4 Energy transfer and dissipation 41
4.1 Energy transfer in MHD 43
4.1.1 Code verification 44
4.1.2 Results: Total energy through the magnetopause in MHD 45
4.1.3 Energy transfer locations in MHD 47
4.2 Energy dissipation in MHD 48

5 Discussion and future directions 52

6 Appendix 56

References 56

1 Introduction

1.1 Structure of the magnetosphere

The existence of the Earth's magnetic field is best known from the alignment of the compass needle. Near the Earth's surface the magnetic field geometry is dipolar, as if it was created by a large bar magnet inside the Earth. Further away from the Earth's surface the dipole field interacts with the plasma of solar origin (the solar wind) and magnetic field it carries (interplanetary magnetic field, IMF). As first considered by Chapman and Ferraro (1931a,b), the dipole magnetic field geometry interacting with the solar wind can be described using the mirror field method, in which a conducting plane representing the solar wind is replaced by an image of the dipole located symmetrically with respect to the plane (Figure 1.1a). The mirror method yields the instantaneous field geometry on the right hand side (in Figure 1.1a) of the conducting plane. However, as the solar wind is advancing typically with a velocity of ∼400 km/s, the solar wind bends around the dipole field forming a bullet-shaped plasma cavity, the magnetosphere[1], as depicted in Figure 1.1b.

The boundary separating the magnetosphere from the solar wind is called the magnetopause (the thick dashed line in Figure 1.1b). Furthermore, as the solar wind streams at a much higher speed than that at which information is conveyed within the plasma, a shock front develops around the magnetopause, similarly to water in a river where a rock sticks out to the surface. The bow shock (thin dotted line in Figure 1.1b),

[1]Chapman and Ferraro thought that the Sun would burst conducting matter only occasionally, so that the magnetosphere would only occasionally be confined by matter originating from the Sun.

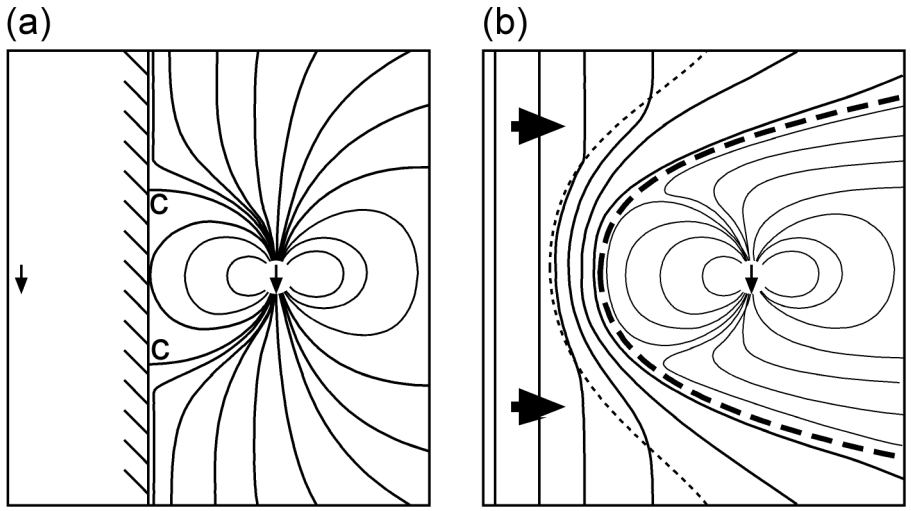

Figure 1.1. (a) Disturbed dipole field geometry in the mirror method. After Chapman and Bartels (1940). (b) Formation of the bullet-shaped magnetosphere in the moving solar wind.

separates the undisturbed solar wind from the shocked solar wind, the magnetosheath. The solar wind compresses the magnetosphere at the sunward side, so that the dayside magnetopause is located roughly at 10 Earth radii[2] distance from the center of the Earth. In the nightside, interaction with the solar wind stretches the magnetosphere forming a long tail (hundreds of R_E's).

Although the mirror field method was the first step in describing the Earth's magnetic field geometry in space, some of its predictions are still valid. For example, a current system develops on the magnetopause, with a purpose of shielding out the magnetospheric magnetic field from the solar wind. These currents are today called the Chapman-Ferraro currents. Furthermore, the mirror analogy yields two singular field lines, labeled with C in Figure 1.1a. Because plasma can freely move along magnetic field lines, these singular field lines mapping to the magnetopause thus offer a location where the magnetosheath matter can enter the magnetosphere. These field lines mark the magnetospheric cusp regions, although in reality the cusps are more like horns of finite width rather than singular field lines.

Figure 1.2 shows a schematic diagram of several regions with different physical conditions within the Earth's magnetosphere. From about 80 km upwards, the Earth's atmosphere is partly ionized due to the extreme ultraviolet (EUV) radiation from the Sun; this upper part of the atmosphere is called the ionosphere. The ionosphere is one of the plasma sources to the magnetosphere, and consequently the near-Earth region ($\sim$1000 km up to $\sim$3-5 R_E) is occupied by cold ($\sim$1 eV) and dense ($\sim 10^3$ cm^{-3}) plasma of ionospheric origin called the plasmasphere. Roughly in the same location as the cold and dense plasmasphere reside the radiation belts, which consist of high-energy (up to GeV's) charged particles. Under the Lorentz force, a charged particle in a magnetic field gyrates around the guide field line. Towards a converging magnetic field, a particle moving along a field line loses velocity parallel to the magnetic field, whereas the velocity component perpendicular to the magnetic field increases; this is due to the conservation of the first adiabatic invariant, the magnetic moment. At the mirror point, the particle has lost all its parallel velocity to the perpendicular velocity component, and thus it bounces back. In the Earth's dipole field configuration, charged particles bounce back and forth between the two mirror points of the dipole, and therefore the particles are trapped in the radiation belts. If the mirror point resides deep enough within the dense atmosphere, collisions due to atmospheric particles may scatter the particles from their bouncing orbits, in which case they precipitate into the ionosphere. The precipitation of charged particles into the atmosphere causes the vivid displays of auroras as the atmospheric particles release the energy they gained from the collisions between the charged particles in the form of light.

A gradient as well as curvature of the magnetic field leads to particle drift motions. Therefore, the gradient in the Earth's magnetic field introduces drifts to the radiation belt particles. As the gradient drift causes the oppositely charged particles to drift in opposite directions, a net current, carried mainly by ions due to their larger energy density, is developed at the magnetic equator. Figure 1.2 shows this intense, roughly toroidal ring current at the Earth's equator ranging from about 2 to 6 R_E (marked with

[2] 1 R_E = 1 Earth's radius, $\sim$6371,2 km

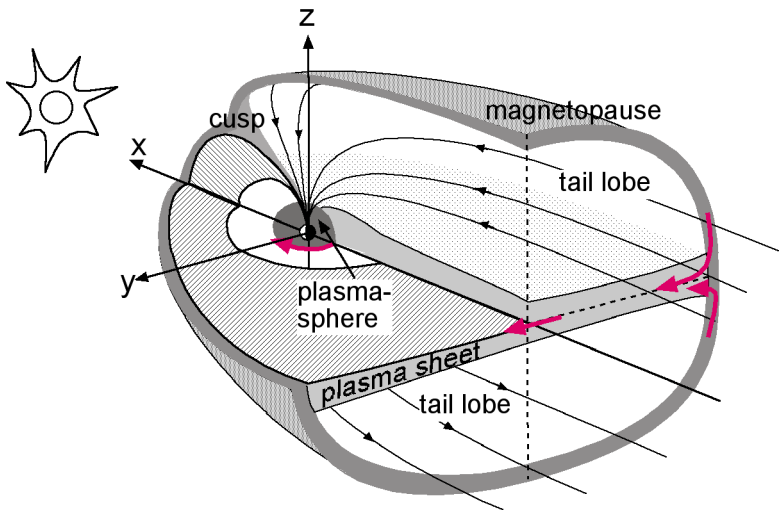

Figure 1.2. A sketch of the different regions within the Earth's magnetosphere.

a red arrow close to the Earth). Furthermore, as the magnetic field lines stretch to form the tail, they are aligned antiparallel to each other in the northern and southern tail lobes. The antiparallel directed magnetic field geometry requires a cross-tail current flowing from dawn towards dusk (marked with red arrow in Figure 1.2), and closing to the magnetopause current system. The cross-tail current flows in the plasma sheet, which is occupied by hot (typically kilovolts) and denser ($\sim$0.1-1 cm^{-3}) plasma.

1.2 Energy transfer mechanisms

Once the existence of the magnetosphere was accepted it was long thought that the solar wind would only encompass the magnetosphere and there would be no interaction between the solar wind and the magnetosphere. Namely, Alfvén (1943) showed that if the plasma is highly conducting, the magnetic field is frozen-in to the motion of the plasma. Inversely, this means that plasma confined by one magnetic field cannot escape to another magnetic field without a major reconfiguration process. Already in the 18th century it was suggested that the solar activity affects the magnetic variations on the ground as large auroral displays and large variations in the Earth's magnetic field occurred in concert with an increasing number of sunspots. Still much later, while the linkage between the active Sun and the ground disturbances was known, it was not understood how the solar wind energy would be transferred through the Earth's dipole field, which, by Alfvén's frozen-in condition, was supposed to act as a shield to the solar wind.

1.2.1 Magnetic reconnection

The concept of magnetic reconnection has been studied since the 1940's, when it was first proposed to be the mechanism which breaks the frozen-in condition and causes heating

and acceleration of plasma in solar flares. Magnetic reconnection basically means reconfiguration of two different magnetic field topologies in which plasma elements that are initially connected to one magnetic field become attached to another magnetic field. As categorized by Priest and Forbes (2000), there are basically two approaches in studying the breaking of the frozen-in condition: While the other concentrates on finding a mechanism that produces large enough resistivity to the plasma to create the necessary dissipation (based on plasma kinetic effects), the other focuses in finding a geometrical configuration that allows the rapid dissipation to take place (the MHD approach). In the following, the basic scenario concerning the latter mechanism is introduced.

Figure 1.3a presents a scenario of two oppositely directed magnetic fields at rest. The field geometry yields a magnetic field gradient between the oppositely directed field lines, which, by Ampère's law creates a current sheet (grey area in Figure 1.3). The induction equation

$$\frac{\partial \mathbf{B}}{\partial t} = \nabla \times (\mathbf{v} \times \mathbf{B}) + \frac{1}{\mu_0 \sigma} \nabla^2 \mathbf{B}, \tag{1.1}$$

where $\mathbf{B}$ is the magnetic field, $\mathbf{v}$ is the bulk velocity of the plasma, and σ is the conductivity, states that the magnetic field changes in time because of convection and diffusion: The field lines convect with the plasma and the field diffuses with respect to the plasma trying to smooth out local inhomogeneities. In a steady state when the plasma does not move (Figure 1.3a), the magnetic field change in time is governed by diffusion: The magnetic field lines annihilate through diffusion, trying to decrease the steep magnetic gradient at the center of the current sheet. While the magnetic field is destroyed in the current sheet, the plasma elements attached to the field lines cannot vanish, instead they gain the energy lost by the field in the annihilation process and are heated. Figure 1.3b represents convection without diffusion: the frozen-in condition holds and the moving field lines pile up at the center of the current sheet and steepen the magnetic gradient, strengthening the current sheet as well.

The reconnection process (Figures 1.3c and 1.3d) requires both convection and diffusion processes: Initially the oppositely directed field lines convect towards each other creating the current sheet between them. The convection of the field lines also creates an electric field, which is the stronger the faster the magnetic field convects towards the current sheet. In the current sheet, the field lines diffuse, and in the process they may form an X-type neutral line (or X-line for short), breaking and reconnecting the field lines as depicted in Figure 1.3d. A current sheet that is thin enough and has a suitable geometry may reconnect spontaneously due to an instability process, e.g., Furth et al. (1963) suggested the ion tearing mode instability. Otherwise the process by which the field lines are broken and reconnected can be thought as driven, i.e., the current sheet reacts to the external boundary conditions. The reconnection process converts magnetic energy into thermal energy, and as two initially unrelated field configurations are connected, their plasma populations are also mixed. The reconnected field lines in Figure 1.3d are subjected to a $\mathbf{j} \times \mathbf{B}$ force which tries to straighten them (upwards and downwards) and in the process the plasma is accelerated (which is sometimes called the slingshot effect).

The original reconnection model put forth by Sweet (1958) and Parker (1957)

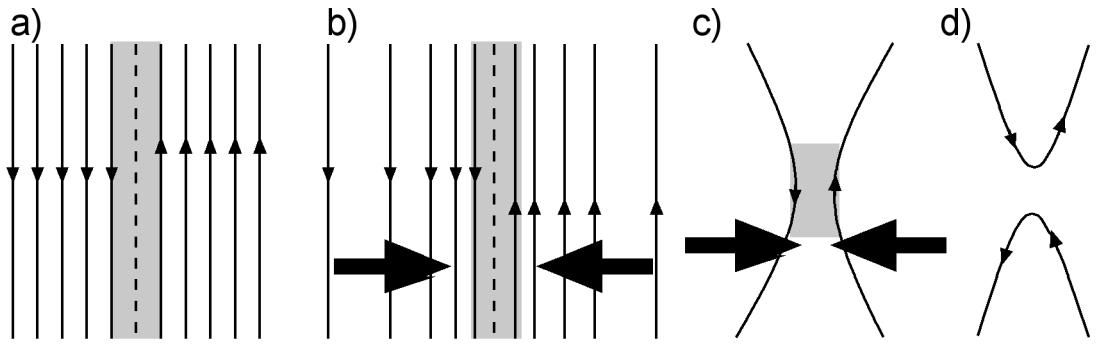

Figure 1.3. a) Field line diffusion and b) convection in the oppositely directed field configuration. c) Formation of the diffusion region between the oppositely directed field lines approaching each other, and d) reconnected field lines.

associated the diffusion region with a finite current sheet between the oppositely directed magnetic field lines. In the Sweet-Parker model, the rate at which the field lines are broken, reconnected and carried away from the reconnection region (the reconnection rate) is equal to the speed at which the field lines are carried to the reconnection region. However, reconnection was introduced to explain the solar flare eruptions, which are considerably faster than the reconnection rate in the Sweet-Parker model.

A new reconnection model providing faster reconnection rates was introduced by Petchek (1964). The size of the long diffusion region in the Sweet-Parker model was shortened, which increased the rate at which the field lines are diffused and reconnected. Furthermore, Petchek realized that the diffusion region emits waves and can thus behave as an obstacle to the plasma inflow, and therefore shock fronts can develop at both sides of the reconnection region. As shocks are known to accelerate particles (for a review, see e.g., Jones and Ellison, 1991), all the particles need not to go through the diffusion region to gain energy: they can be accelerated at the shocks. Petchek's model is fast enough to account for the solar flare eruptions, and as will be discussed further, there is also observational evidence of the Petchek-type reconnection taking place within the magnetotail.

The first application of the reconnection theory to the solar wind - magnetosphere system was proposed by Dungey (1961), who suggested that during southward IMF reconnection would take place at the dayside magnetosphere between the IMF and northward oriented terrestrial magnetic field. Figure 1.4 illustrates global circulation set up by dayside reconnection in Dungey's model. Initially, the southward IMF advancing towards the Earth reconnects with the dipole field line creating an "open" field line whose other end is attached to the Earth and the other to the solar wind. The newly reconnected field line (marked with 1 in Figure 1.4a) is highly bent, and thus on one hand a $\mathbf{j} \times \mathbf{B}$ force tries to straighten it, and on the other hand it is dragged tailwards over the polar cap (2-5) with the solar wind flow. Naturally the other part of the reconnected dipole field line attached to the southern polar cap experiences a similar evolution. In the distant tail, the additional magnetic flux forces the field lines to move towards the equatorial plane, and as the northern and southern open field lines are now

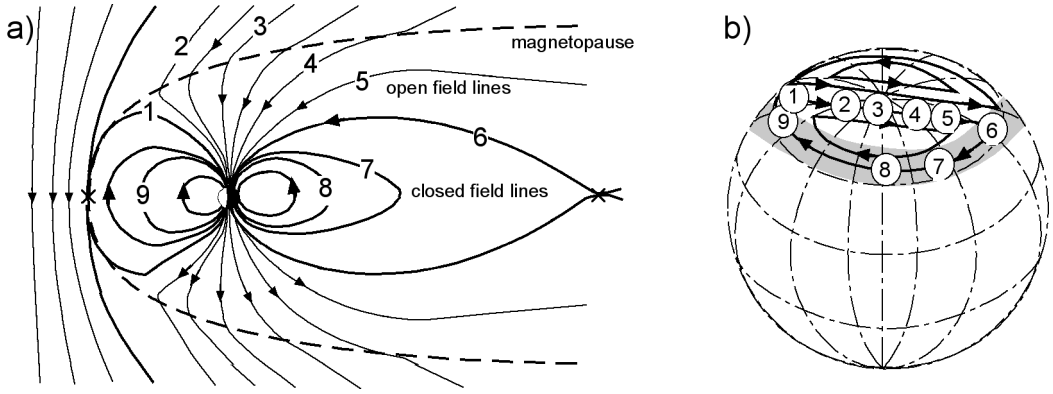

Figure 1.4. Reconnection and field line convection a) in the magnetosphere and b) in the ionosphere. After Dungey, (1961).

oppositely directed, reconnection will occur again. The two open field lines merge again forming a closed field line (6), which then returns to the dayside (7-9). As the field lines are (almost) equipotentials, the motion of the field lines maps to the ionosphere (Figure 1.4b) and establishes global convection cells, with tailward flow within the polar cap and sunward flow in the lower latitudes.

Dungey's model gives new significance to the magnetospheric configuration. For example, in Dungey's model the cusps are no longer caused by the static presence of conducting matter outside the magnetopause. Rather, the cusps are opened because of reconnection, during which they are regions originating from the interaction between the solar wind and the magnetosphere. However, their original role as locations where solar wind matter can freely enter the magnetosphere still holds. Another new meaning can be given to the tail lobes introduced in Figure 1.2, because they map to the polar cap and hence they are regions consisting of open field lines. The boundary of open and closed field lines in the tail, the plasma sheet boundary layer, maps to the poleward edge of the auroral oval (gray-shaded area in Figure 1.4b) in the ionosphere. Furthermore, the circulation of plasma along with the field lines creates field-aligned currents flowing between the ionosphere and the magnetosphere; these field-aligned currents are also links between the magnetosphere and the ionosphere. Region 1 field-aligned currents flow to the ionosphere in the morning sector and away from the ionosphere in the evening sector. Region 2 field-aligned currents exist equatorward of the Region 1 currents and they flow in the opposite direction to Region 1 currents, closing to the inner magnetosphere. Additionally, the net downward field-aligned currents feed auroral horizontal electrojets that flow eastward (westward) in the dusk (dawn) region (e.g., Kamide and Baumjohann, 1993).

While Dungey (1961) considered only southward IMF in his model, reconnection between the IMF and terrestrial magnetic field can occur with a variety of different IMF orientations. Basically any IMF direction can produce reconnection provided that the terrestrial field is opposite to the IMF and that there is enough convection of plasma towards the field reversal region to bring the two field configurations in contact. In particular, the IMF B_z plays a major role on the reconnection efficiency: During southward

IMF the solar wind and terrestrial fields are easily reconnected and hence during southward IMF the energy input to the magnetosphere is particularly enhanced. IMF B_y, on the other hand, plays a major role in determining where reconnection occurs (e.g., Luhmann et al., 1984). The convection pattern is deflected from the noon-midnight meridian due to the y component of the IMF[3]. Reconnection at the distant neutral line in the magnetotail is present also during geomagnetically quiet times (Nishida et al., 1994), i.e., during times when the IMF B_z is northward. Under these conditions, the dayside reconnection occurs poleward of the cusp at the high latitude dayside magnetopause. Consequently, global convection is continuously present, although it is weaker during northward IMF. As the IMF encompasses the magnetosphere the IMF B_x component changes into y- and z-directed magnetic field in the magnetosheath (Kallio and Koskinen, 2000), and therefore also IMF B_x has an influence on the location where the reconnection occurs at the magnetopause.

Qualitatively, Dungey's model describes the dependence of the global dynamical processes on the IMF direction. Quantitative observational assessment of the reconnection process can be made either directly by *in situ* measurements or indirectly by observing dynamics set up by reconnection. Given the large size of the magnetosphere, the rendezvous of a spacecraft with the reconnection diffusion region is quite improbable. Nonetheless, Ho et al. (1994) reported of a fortunate event in the distant tail recorded by the ISEE-3 satellite. A reconnection region fly-by was evidenced by a pair of Petschek-type shocks on both sides of the X-line, which itself was signified by the reversal of the B_z component. Fast plasma flows earthward and tailward were also observed, completing a collection of independent evidence of reconnection.

The global dynamics set up by dayside reconnection has several manifestations and therefore the reconnection efficiency can be estimated also in many indirect ways. While the onset of dayside reconnection triggers an enhancement of global convection, the return flux from the nightside reaches the dayside with a time delay leading to erosion of the dayside magnetopause until steady state is attained. The magnetopause location on the other hand can be measured with satellites (e.g,. Fairfield, 1971). Furthermore, the plasma flow in the solar wind is associated with an electric field ($\mathbf{E} = -\mathbf{V} \times \mathbf{B}$), and as the reconnected magnetic field lines are almost equipotentials, the interplanetary electric field (IEF) produces a measurable electric potential difference over the open field line region, the polar cap potential. Thus also the reconnection efficiency is related to the polar cap potential (e.g., Reiff et al., 1981). As the open field lines map to the polar cap, the polar cap size is a measure of the amount of magnetic flux within the tail lobes. At times when dayside reconnection adds a large amount of new flux to the polar cap and tail lobes, the boundary of open and closed field lines moves equatorward along with the auroral oval. The shift of the auroral oval location is then an indicator of the imbalance between the dayside reconnection rate and the nightside convection integrated in time. Hence, correlations of the oval size and location to the solar wind parameters contain natural scatter caused by the time history of the solar wind parameters.

[3]also Hall conductivity causes the deflection of the convection pattern, (Kamide and Baumjohann, 1993)

1.2.2 Other energy transfer mechanisms

The reconnection process transfers energy, mass, and momentum to the magnetosphere most efficiently when the IMF is southward and thus opposite to the terrestrial field at the dayside. Northward turning of the IMF reduces reconnection in the dayside magnetosphere, but the energy transfer process from the solar wind into the magnetosphere is never completely halted even during northward IMF. For instance, the polar cap potential does not reach zero even during prolonged times of northward IMF, but settles to about 35 kV (Reiff et al., 1981). This indicates that there are background energy, mass and momentum transfer processes that are active at all times. Furthermore, a layer of magnetosheath-like plasma (low-latitude boundary layer, LLBL) just inside the magnetopause, as well as a layer of magnetosphere-like plasma just outside of the magnetopause (the magnetosheath boundary layer, MSBL) are commonly observed under all IMF conditions (e.g., Hones et al., 1972; Meng and Anderson, 1970). Energy, mass and momentum transfer processes other than reconnection are collectively called viscous interaction processes, a term first proposed by Axford and Hines (1961).

The charged particles gyrate around the magnetic field line under the Lorentz-force (Larmor motion). Collisions between particles can scatter the gyrating particles off their field lines, leading to increased cross-field diffusion. In tenuous space plasmas classical collisions are rare; however scattering of particles can also be provided by means of wave-particle interactions (diffusion originating from other mechanisms than classical collisions is called anomalous diffusion). The strongly fluctuating wave field providing particle scattering needs free energy, which can be released e.g., through a plasma micro-instability such as the lower-hybrid drift instability[4] (e.g., Sibeck et al., 1999). On the other hand, macro-instabilities, such as eddy turbulence or Kelvin-Helmholtz instability[5], provide the background motion for the micro-instabilities (e.g., Sibeck et al., 1999). Furthermore, the intense wave fields can have the same frequency as the particle gyro-motion; the resulting pitch-angle scattering can be very efficient in kicking particles away from their Larmor orbits (Tsurutani and Thorne, 1982). One important aspect of diffusion is also to realize that a finite resistivity by definition breaks the frozen-in condition. Therefore the existence of an instability that leads to wave fluctuations that scatter particles and therefore results in diffusion can ignite the reconnection process if the circumstances are otherwise favorable, i.e., there is plasma convection towards the diffusion region and the magnetic fields in both sides of the magnetopause are antiparallel to each other.

The Larmor radius of the gyro-motion of particles around the magnetic field line depends on the particle mass and energy, such that lighter particles gyrate with a smaller radius, whereas increasing particle energy increases the gyro-radius. For example, the Larmor radius of magnetosheath ions having energies above the thermal speed is of the order of or greater than the magnetopause scale size, and thus they may cross the magnetopause current layer while gyrating around their specific field lines (e.g., Stasiewicz,

[4]Lower-hybrid drift instability arises from the resonance of the lower-hybrid mode and the plasma drift velocity.

[5]Kelvin-Helmholtz instability (KHI) arises from the shear in the flow velocities across the magnetopause, and is capable of producing surface waves along the magnetopause.

1994). Furthermore, the curvature and the magnetic gradients at the magnetopause may be involved in allowing particle entry inside the magnetopause, if the gradient and curvature drifts are directed towards the magnetopause (e.g., Olson and Pfitzer, 1985). Therefore, some energetic particles may simply drift across the magnetopause under the influence of the magnetic field gradient and curvature at the magnetopause. Particle entry mechanisms related to the finite Larmor radius are collectively called the finite Larmor radius (FLR) effects.

A possible particle entry mechanism across the magnetopause is related to the $\mathbf{E} \times \mathbf{B}$ drift. As the terrestrial magnetic field is directed northward at the subsolar magnetopause, a plasma blob exposed to a dusk-to-dawn directed electric field in the Earth's rest frame would drift across the magnetopause to the magnetosphere (e.g., Lemaire, 1977), this is often called impulsive penetration. Such electric fields could be generated e.g., due to difference in the ion and electron gyroradii, such that the charges could separate and generate a polarization electric field.

Finally, regarding mass, energy and momentum transfer from the solar wind into the magnetosphere, special attention must be paid to the cusp regions, as already noted by Chapman and Ferraro (1931a,b). The solar wind matter enters the magnetosphere via the cusp field lines, along which particles gyrate earthward in the cusp's converging field topology. At low altitudes, the charged particles mirror and begin to flow away from the Earth. At the same time the open field line is dragged through the cusp. This leads to a situation where particles originally attached to a dayside field line change to a nightside field line within the cusp due to the $\mathbf{E} \times \mathbf{B}$ drift. This indicates that the nightside lobes are also partly populated via the cusps (Rosenbauer et al., 1975).

1.3 Practical significance

The energy transfer process between the solar wind and the magnetosphere and further between the magnetosphere and the ionosphere is one of the key questions in space physics. Magnetospheric dynamics is largely controlled by the external driver, the solar wind and its magnetic field. Internal magnetospheric processes contribute to the details of the magnetospheric dynamics, but the energy required to power the system is drawn from the interaction with the solar wind, especially during periods of southward IMF (e.g., Baker et al., 1997). Qualitatively, the energy input is explained by the magnetopause reconnection (Dungey, 1961) and viscous interaction (Axford and Hines, 1961), but quantitative assessment of the problem has proven to be difficult. Therefore, reliable estimates on the amount of transferred and dissipated energy within the magnetosphere are listed as top open questions in international space physics programs, such as the International Solar Terrestrial Program (ISTP), as well as in individual satellite mission programs, such as the Cluster mission of the European Space Agency (ESA).

Understanding of the space environment has gained more interest in the past few years, as an increasing amount of technologies, such as communication systems, depend on space environment. A new applied discipline, termed space weather, has emerged within the solar - terrestrial sciences (e.g., Carlowicz and Lopez, 2002), which deals with a long list of harmful effects to man-made systems ultimately caused by the Sun.

For example, solar outbursts of high energy particles are a threat to humans working in space, furthermore they are known to cause malfunctions or even failures of spacecraft, which may hamper e.g., communication systems at Earth. The high energy particles within the radiation belts are a threat to satellites residing in this region. The rapidly changing ionospheric current systems induce rapidly changing magnetic fields, which in turn induce geoelectric fields to the ground. The geoelectric field drives geomagnetically induced currents (GIC) in long conductors, such as power grids, natural gas pipelines and railway lines (e.g., Boteler et al., 1998) predominantly at high latitudes. At low latitudes, geomagnetic activity causes trouble e.g. in satellite - ground communication links owing to a phenomenon called the equatorial spread-F (e.g., Palmroth et al., 2000), which is essentially ionospheric density depletion through which the satellite signals may be deteriorated.

1.3.1 Scope of this thesis

A thorough understanding of the linkage between the Sun and the surface of the Earth and all the physical phenomena occurring in between is essential in trying to predict space weather. As the energy from the Sun fuels almost all the dynamical processes in the near-Earth space, the energy coupling between the solar wind and the magnetosphere is at the heart of the effort in putting forth a reliable prediction of the space environment. Research topics actively investigated include a realistic estimation of the total amount of energy transferred into the magnetosphere, the location of where significant energy transfer occurs, the actual mechanism that leads to the transfer of energy, locations where energy is consumed within the magnetosphere and ionosphere, and the relative importance of the various energy sinks. This thesis investigates the aforementioned questions by presenting the two main dynamic processes of the magnetosphere, magnetic storms and magnetospheric substorms as manifestations of the energy transfer processes. Furthermore, the special role of the cusp is also investigated in light of the solar wind - magnetosphere interaction. In particular, this thesis introduces new methods of estimating the energy transfer rate as well as identifying the energy transfer locations by using numerical simulations. The numerical simulations are also used in calculating the ionospheric energy dissipation, which gives insight to the relative importance of the different ionospheric energy sinks. Finally, the quality of the results obtained by the numerical simulation is discussed and compared to results obtained by other methods.

2 Manifestations of energy transfer: Magnetospheric dynamics

2.1 Cusp dynamics

The two spatially narrow cusps in the dayside magnetosphere are regions where the magnetosheath particles have a direct access to the magnetosphere and the ionosphere (e.g., Heikkila and Winningham, 1971; Newell and Meng, 1988; Smith and Lockwood, 1996). While nominally the cusp lies around local noon near 75°- 80° latitude, the location of the cusp both in latitude as well as in local time is strongly dependent on the solar wind and IMF conditions (e.g., Burch, 1973; Newell et al., 1989). The location of the cusp thus gives information of the state of the magnetosphere and of the solar wind control of the magnetosphere. As the cusps are closely related to reconnection at the magnetopause, the cusp location and properties also provide information on the magnetopause reconnection location.

It is widely accepted that the IMF B_z is the main controlling factor of the cusp latitude (Burch, 1973; Smith and Lockwood, 1996). Larger southward IMF B_z component eliminates a larger portion of the magnetopause due to reconnection, moving the magnetopause earthward and the cusp to lower latitudes. During increasing northward IMF the cusp location is fairly stationary or moves slightly poleward (e.g., Newell et al., 1989). The peak probability of observing the cusp shifts to the prenoon sector for negative (dawnward) B_y, and to the postnoon sector for positive (duskward) B_y in the Northern Hemisphere, in the Southern Hemisphere the shift is in the opposite direction (Newell et al., 1989). This behavior results from the fact that a dawnward IMF B_y shifts the reconnection site dawnward in the Northern Hemisphere and duskward in the Southern Hemisphere (e.g., Luhmann et al., 1984; Kallio and Koskinen, 2000). The spatial extent of the cusp also varies with the solar wind conditions. A prolonged northward IMF widens the cusp latitudinally, whereas during southward IMF the cusp is usually narrow in latitude (e.g., Newell and Meng, 1987).

Observationally, the cusp has several signatures from which it can be identified. One of the most widely used ways of identifying the cusp is the ion energy-latitude dispersion measured at polar low Earth orbit satellites (e.g., Rosenbauer et al., 1975). During low-latitude magnetopause reconnection the high-energy ions reach the ionospheric footprint of the reconnection region at lower latitudes but as the field line convects poleward through the cusp, the low-energy ions appear later only at higher latitudes. However, during northward IMF, when reconnection is expected to take place at the boundary of tail lobes (e.g., Luhmann et al., 1984) and the resulting global convection is sunward, the high-energy ions reach ionospheric footprint of the reconnection region at higher latitudes, whereas the low-energy ions are convected to lower latitudes with the open field line (e.g., Topliss et al., 2000). Another way to discern the cusp is by diamagnetic depression (e.g., Tsyganenko and Russell, 1999), i.e., a decrease of the total magnetic field as a result of the incoming magnetosheath particles. The entry of the magnetosheath particles is also seen as enhanced plasma density.

Paper I of this thesis investigates statistically the solar wind control of the cusp

location and its latitudinal extent using the Polar satellite data. The cusp is identified from the spacecraft potential measurement, a quantity related to the plasma density. Owing to the entry of the magnetosheath particles, the cusp shows as a density enhancement. By using the Polar spacecraft potential measurements from April 1996 to May 1999, we created a data set containing each Polar pass across 80° between 0900 and 1600 MLT, yielding a total of 396 events.

As illustrated in many papers (e.g., Newell et al., 1989; Zhou et al., 2000), the cusp latitude information contains a large amount of scatter when plotted against the IMF B_z. In particular, Paper I concentrates on the sources of scatter in the cusp latitude. Paper I lists major sources of scatter (dipole tilt, mapping errors, cusp motion, magnetosheath fluctuations, IMF B_y effect) in the cusp latitude and evaluates their relative importance: First the events were carefully selected, after which the remaining events were regrouped by the possible mechanisms causing scatter in the cusp latitude. The method outlines the major source of scatter in the cusp latitude, and thus it determines the components in the solar wind that mainly affect the cusp location.

After the attempt to eliminate errors in the cusp latitude due to dipole tilt, mapping errors, and cusp motion (Paper I), 46 events were left of the initial data set containing 396 events. The 46 events appeared in between 1000 and 1409 MLT. The scatter in the cusp latitude was significantly diminished, which can be seen by comparing Figures 5 and 6 of Paper I. However, the correlation between the cusp latitude and the IMF B_z was still quite poor. The remaining outliers (Figure 6 of Paper I) were attempted to explain with scatter sources due to magnetosheath fluctuations and the IMF B_y effect.

Magnetosheath fluctuations have been proposed to trigger transient ionospheric events related to dayside reconnection (Newell and Sibeck, 1993), and they may also cause magnetopause motion (Sibeck and Gosling, 1996). As the dayside magnetopause maps to the cusp and the cusp is closely related to dayside reconnection, we tested a hypothesis that magnetosheath fluctuations could affect the cusp location. The magnetosheath fluctuations usually follow solar wind pressure pulses or fast IMF fluctuations. However, as the events were already selected during steady IMF B_z and solar wind dynamic pressure conditions, we determined the probability that the magnetosheath was turbulent during the events using IMF measurements. Namely, the IMF is known to precondition the magnetosheath flow such that in the sector where IMF is perpendicular to the shock normal (known as a quasi-perpendicular shock) the flow is quite smooth, whereas in the sector where IMF is parallel to the shock normal the flow is usually turbulent (known as a quasi-parallel shock) (e.g., Greenstadt et al., 1984). Therefore, we determined using IMF measurements whether the dayside subsolar magnetosheath was probably smooth or turbulent, corresponding to quasi-perpendicular and quasi-parallel shock, respectively. The classification of the events to the quasi-parallel and quasi-perpendicular categories diminished the scattering of the cusp latitude to some extent, such that events during a probably smooth magnetosheath (quasi-perpendicular events) were not as scattered as the events during a probably turbulent magnetosheath (quasi-parallel events). However, we conclude that the possibility of the magnetosheath fluctuations affecting the cusp location must be investigated based on *in situ* measurements of the magnetosheath instead of relying on the probability of the smoothness/turbulence

of the magnetosheath based on IMF measurements only.

The IMF B_y has a strong influence on the reconnection site (e.g., Luhmann et al., 1984; Kallio and Koskinen, 2000) and thus it has an influence also to the cusp location. We tested the IMF B_y effect by classifying the 46 events once more such that only events with a small average IMF B_y were considered. During small IMF B_y the cusp is likely to be located near the local noon, and thus Polar is likely to move through the center of the cusp. The restriction to events during which the average of IMF B_y is small reduced the scattering between the cusp latitude as a function of the IMF B_z: During southward IMF only one outlier existed and the correlation was over 90% for both the poleward and equatorward boundaries. During northward IMF the correlation was at best 63% on the poleward boundary (cf. Figure 7 of Paper I). However, the average of IMF B_y is small when, e.g., the IMF B_y fluctuates from a large positive value to a large negative value, and therefore we searched for large fluctuations of IMF B_y in each event individually. The anomalous outlier during southward IMF was the only one with largely fluctuating IMF B_y, however during northward IMF there were several events with fluctuating IMF B_y. The fluctuation of the IMF B_y seems to have a larger effect on the cusp latitude when the IMF is southward than when it is northward. The 7-nT fluctuation of IMF B_y in the anomalous event influences the cusp latitude by several degrees when the IMF is southward, yet similar fluctuation of IMF B_y during northward IMF does not shift the cusp latitude as dramatically. Therefore we conclude that the largest source of scatter in the cusp latitude is due to both large as well as highly fluctuating IMF B_y, especially during southward IMF when the cusp is already sensitive to the solar wind variations. Paper I further concludes that the high-altitude cusp is located $\sim 2^\circ$ poleward of the low-altitude cusp (Newell et al., 1989). This discrepancy is due to mapping uncertainties, which also add scatter to cusp location as invariant latitude mapping contains systematic errors particularly when mapping from high altitudes.

The sources of scatter in the cusp location as a function of IMF B_z may include also the cusp identification method itself and the possible effect of the previous state of the magnetosphere, i.e., a "magnetospheric memory" effect. As these issues cannot be addressed with the data set in Paper I, they were later dealt with in Paper III. The effect of the different identification methods was considered by comparing the cusp boundaries identified from Polar spacecraft potential data to cusp boundaries identified with ion energy-latitude dispersion signature. The result was that the cusp boundary closer to the reconnection site was more easily detected and thus more likely in the same place in both identification methods. Therefore, for southward (northward) IMF the particle signatures and the density enhancement are at the same place at the equatorward (poleward) boundary of the cusp. However, the boundary further away from the reconnection site was more vague and thus more likely to add statistical noise to the boundary determinations.

2.2 Magnetospheric substorms

A fundamental dynamical sequence in which the magnetosphere first loads and then unloads solar wind energy is termed a substorm. While the author has not primarily investigated substorms, the following describes briefly the substorm sequence as it is understood at present, because the dynamics involved in substorms are key elements in understanding magnetospheric behavior under the solar wind driver.

McPherron (1979) defines the substorm as "...a transient process initiated on the nightside of the Earth in which a significant amount of energy derived from the solar wind - magnetosphere interaction is deposited in the auroral ionosphere and magnetosphere." The first model of a magnetospheric substorm (Akasofu, 1964) included two phases, the expansion phase and the recovery phase. Later, McPherron (1970) added a third phase, the growth phase, to the substorm sequence. Figure 2.1 depicts the different phases. Usually, a southward turning of the IMF marks the beginning of the growth phase. Following Dungey's (1961) reasoning, new magnetic flux is thus being added to the tail lobes, which both stretches the tail (Figure 2.1b) as well as moves the auroral oval equatorward. The tail stretching can be observed by the increase of the B_x-component and decrease of the B_z-component of the magnetic field as recorded by satellites traversing the nightside magnetosphere. As the auroral oval moves equatorward, a quiet eveningside auroral arc mapping to the plasma sheet moves slowly equatorward. Also the intensity of the ionospheric horizontal currents gradually increase leading to a gradual increase of the AE index[1].

New magnetic flux added to the tail lobes during the growth phase stretches the tail and consequently compresses the plasma sheet (Figure 2.1b), increasing the intensity of the duskward cross-tail current as well. At present, there are at least two competing scenarios of what happens at the end of the growth phase. According to the near-Earth neutral line model (NENL, e.g., Baker et al., 1996), the current sheet thinning continues during the growth phase until it has the scale size of the thermal ion gyroradius. Under such conditions, the ions are no longer tied to the magnetic field, and ion and electron dynamics become decoupled, which leads to a polarization electric field that allows the cross-tail current intensification within the center of the plasma sheet (e.g., Pritchett and Coroniti, 1995). As discussed earlier, a thin enough current sheet may reconnect, either spontaneously via a plasma instability (e.g., Furth et al., 1963), or as a response to changed boundary conditions, i.e., as a response to external driving, which may include northward turning of the IMF or reduction of the magnitude in the IMF B_y component (Lyons, 1996). Reconnection initiated within the closed field lines in the plasmasheet leads to the disruption of the cross-tail current (Figure 2.1c), which must find a new closure path. This is achieved, when the cross-tail current deviates along field lines to the ionosphere creating an additional westward (duskward) current in the midnight sector. Reconnection in the closed field lines results in plasma being injected from the reconnection region both earthward and tailward. After all closed field lines have been reconnected, a plasmoid is ejected tailward.

[1]Auroral electrojet (AE) index is computed from several roughly uniformly distributed ground stations at the auroral region such that AE is the difference of the upper (AU) and lower (AL) envelopes of the superposed horizontal (H) component.

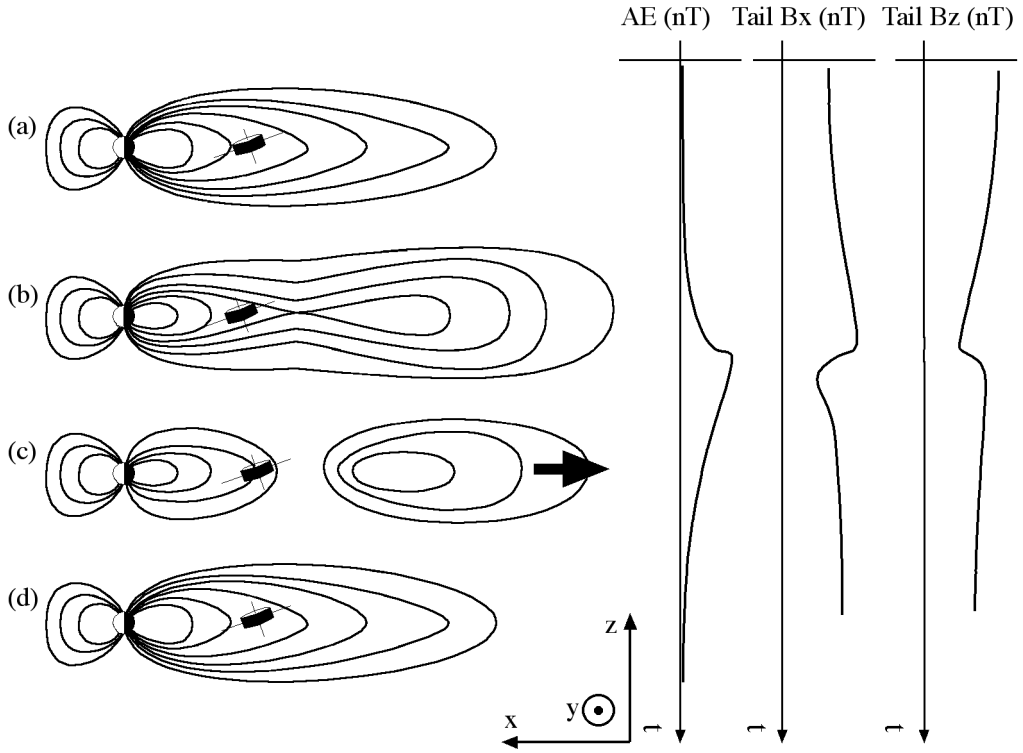

Figure 2.1. (right) a) Magnetosphere at its "ground state", b) growth phase and the beginning of the expansion phase, c) expansion phase and dipolarization, d) return to the ground state. (left) Time series data (arbitrary units) of AE index, and time series data (arbitrary units) of an imaginary satellite located in the tail.

The current disruption model (CD, e.g., Lui, 1996) has a different view on the onset process. In the CD model, a turbulent plasma process in the near-Earth tail on auroral field lines causes a current disruption and sets up the current wedge coupled to the ionosphere. The near-Earth current disruption sends a tailward traveling wave, which leads to current disruptions in multiple locations in the tail, resulting finally in a large scale reconnection process and the launch of a plasmoid. Since the relevant substorm-related issue pertaining this thesis, that substorms load and unload solar wind energy, is independent of the onset model, the selection of which model better explains the terrestrial substorms is not in the scope of this thesis.

The substorm onset is observed as a sudden brightening of the quiet arc that was moving equatorward. The auroral forms expand poleward, eastward and westward. Ground-based magnetometers located below the auroral oval record a sudden intensification of the westward ionospheric current, which is seen as a sudden increase of the AE index. A satellite traversing the tail (see Figure 2.1) records a sudden decrease of the B_x component of the tail magnetic field, since the tail undergoes a change from a stretched topology into a more dipolar topology. Likewise, the B_z component of the tail magnetic field increases in intensity. The tail disruption also involves magnetic pulsations, which travel along the magnetic field lines and are recorded by ground magnetometers. Fur-

thermore, particle detectors onboard a satellite traversing the tail detect the injected particles.

After the dipolarisation, the magnetosphere starts to slowly retain its ground state (Figure 2.1d). A new magnetotail forms when the dipolar field stretches back to its original form. The recovery phase can be observed from ground magnetometers, where the AE index gradually decreases after the sharp increase during the expansion phase, signifying that a decreasing amount of the cross-tail current closes through the ionosphere. The auroral forms have reached their furthest poleward position during the expansion phase, and during the recovery phase they start to move equatorward as the tail stretching advances. The satellites traversing the magnetotail record again an increase of the B_x component, whereas intensity of the B_z component decreases.

2.3 Magnetic storms

A magnetic storm is a term given to a time period during which the global magnetic field, as measured by low-latitude ground magnetometers, significantly decreases (e.g., Chapman and Bartels, 1940). The intensity of the storm can be characterized by the minimum of the Dst index[2] (e.g., Gonzalez et al., 1994), such that during intense storms the global field decreases at least a hundred nT (out of about 30,000 nT ground field at the equator). The interplanetary causes of such long-duration (several days) global magnetic field disturbances have been related to an intense and long-lasting southward IMF associated with the duskward interplanetary electric field (IEF) that is the main driver of global convection in the magnetosphere. For instance, Gonzalez and Tsurutani (1987) define a southward IMF of at least -10 nT for more than 3 hours as a sufficient condition for the development of an intense magnetic storm. Furthermore, Gonzalez and Tsurutani (1987) associate these long-duration and intense IEF enhancements either with high-speed streams or with "solar wind density enhancement events", nowadays known by the term coronal mass ejections (CME). CMEs are large plasma clouds ejected from the Sun and, characterized by intense flux-rope-like magnetic fields and low dynamic pressures. As the CMEs often travel faster than the ambient solar wind, a shock front develops in front of the CME. The interplanetary manifestation of a CME is called an interplanetary CME (ICME). CMEs, particularly those associated with a shock, are regarded as the most important drivers of strong global geomagnetic activity (e.g., Gosling et al., 1991).

A magnetic storm consists of two or three phases: initial phase (not necessarily in all storms), main phase and recovery phase, all identified from the time series of the Dst index (see Figure 2.2). The initial phase, which begins with a storm sudden commencement (SSC), is distinguished as a positive excursion in the ground magnetic field: As the CME hits the magnetopause, the magnetopause is compressed and the Chapman-Ferraro currents are intensified, leading also to the increase of the ground field at the equator (Chapman and Ferraro, 1931a). The storm main phase is characterized both by the rapid decrease of the Dst index as well as the equatorward motion of the

[2]Dst (disturbance storm time) index is defined as the instantaneous average of the disturbance in the equatorial H-component at several low-latitude magnetometer stations.

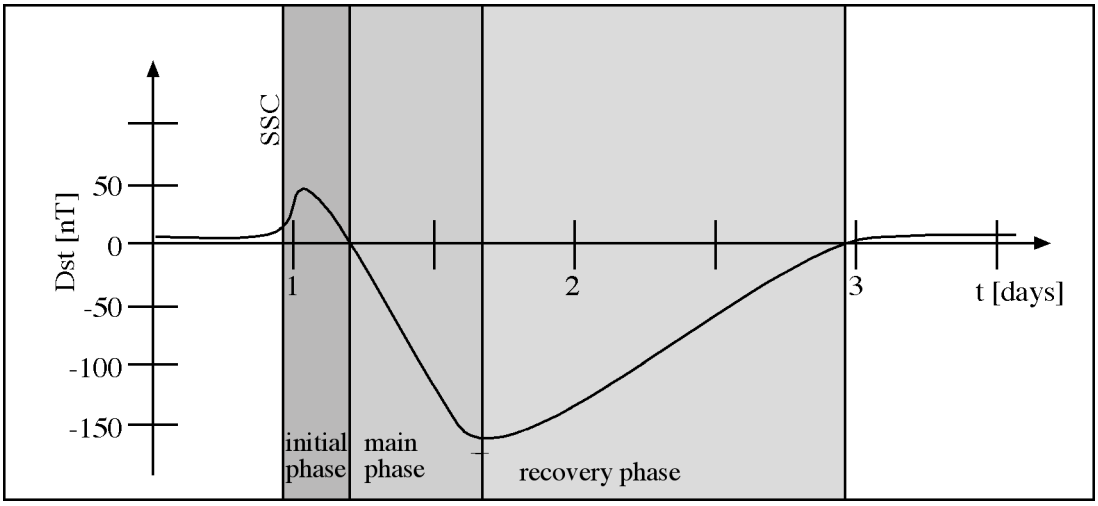

Figure 2.2. Evolution of the Dst index during a magnetic storm.

auroral ovals and occurrence of auroral intensifications and substorms. After the main phase follows the recovery phase during which the Dst index slowly recovers to the level preceding the storm. During the recovery phase the auroral oval returns to its nominal position and the overall magnetic activity subsides.

Although Dst is measured on the ground and is thus affected by all major current systems within the magnetosphere, the decrease of the ground field is mainly caused by the enhancement of the westward flowing ring current (e.g., Singer, 1957; Turner et al., 2001). Two distinct mechanisms for the intensification of the ring current have been suggested. Originally Chapman (1962) suggested that magnetic storms consist of several substorms, in which case the substorm injections are thought as the main contributors to the ring current enhancement (hence the name *substorm*). This view was challenged by e.g., Kamide (1992), who claimed that a substorm occurrence is not a necessary condition for the development of a magnetic storm, and that the injections causing the ring current enhancement are due to the enhancement of the convection electric field driven by the solar wind. This view is supported by the facts that the temporal variation of the Dst index can largely be predicted from the solar wind observations only (e.g., Burton et al., 1975), and that the effects of particles injected and energized by the substorms are undetectable in the Dst index (McPherron, 1997). However, compositional observations have shown that the total energy density of the ring current is dominated by ions of ionospheric origin (O^+) during the storm main phase (e.g., Hamilton et al., 1988; Daglis, 1997). As the abundance of ionospheric ions in the storm-time ring current is associated with ionospheric outflows, which in turn may result from the substorm-associated electric fields (Kamide et al., 1998), the storm-substorm relationship is by no means a resolved issue.

Paper II investigates the chain of events starting from the Sun that led to the development of the second largest magnetic storm in the year 2000 as determined by the minimum of the Dst. The aim of the paper is twofold: First the solar and interplanetary observations were carefully analyzed and secondly, these results were used in a detailed

examination of the magnetospheric response, including the ground effects as manifested by the geomagnetically induced currents. Paper II shows that the 6 April 2000 magnetic storm was driven by the shock of the CME, and that the shock driver gas (the CME ejecta) was not observed until the storm recovery phase. In fact, Paper II presents evidence that the CME swept past the Earth and that the magnetosphere mainly resided in the flank of the shock driven by the CME ejecta. In particular, the 6 April 2000 storm was characterized by an intense interplanetary magnetic field and unusually high pressures, which are both likely to cause pronounced geomagnetic activity. However, previous papers (e.g., Gosling et al., 1991) find that almost all geoeffective storms are driven by the mutual influence of both the CME ejecta and the shock that precedes the driver gas. Therefore, one highlight of Paper II is to demonstrate to space weather forecasters that major magnetic storms can develop solely due to interaction with the sheath region of a CME.

The magnetospheric response to the solar wind driver was determined by using ground magnetometers. As the storm occurred while Fennoscandia was close to the local midnight during the storm main phase, the Fennoscandian IMAGE magnetometer chain was used to determine auroral activations characterized by a negative bay onset of the horizontal ground magnetic field component. Individual magnetometer station recordings were used to determine the direction of propagation of the auroral activations, and geosynchronous particle observations were used to determine whether there were injections accompanying the auroral activations. The outcome was that out of eight auroral activations only four fulfilled the characteristics usually attributed to substorms, i.e., predominantly poleward and westward auroral propagation accompanied with geosynchronous particle injections. Out of these four substorms two involved possible solar wind triggering: One occurred during a strongly oscillating solar wind pressure at a deep minimum of the IMF B_z (and thus during enhanced energy input), and the other followed the final northward turning of the magnetic field. Furthermore, Paper II notes that the high-resolution Dst index (SYM-H index) does not show a correlation to the high-latitude magnetic variations, which lends support to the conclusion that substorms do not play a significant role in the storm evolution as determined from the Dst index (Kamide, 1992). However, final conclusion of the storm-substorm relationship requires a more through understanding of the properties and drivers of all types of electrojet and auroral activations during storms.

3 Global MHD simulations

3.1 The MHD description

Plasma is a quasineutral gas consisting of free charges. Furthermore, as a collection of charges, plasma is highly conducting, and hence electromagnetic fields control the motion and physical behavior of the plasma, particularly in typical tenuous space plasmas, where collisions between particles are virtually nonexistent. Plasmas react collectively to electromagnetic fields, and therefore the plasma behaves as a continuous medium. Whereas Euler and Navier-Stokes equations govern the motion and behavior of non-magnetized fluids (with zero and nonzero viscosity, respectively), the equations describing plasma motions need the effects of magnetic and electric fields. The set of equations that resembles the fluid mechanical description but includes the electromagnetic effects is called *magnetohydrodynamics* (MHD), largely introduced by Hannes Alfvén. In MHD the plasma is treated as a continuous medium described by a single temperature, number density and bulk velocity. In theory, treatment of the plasma as a fluid assumes that the length scale of interest (L) is much larger than the velocity randomizing length. As randomizing mechanisms classical collisions, wave-particle interactions (anomalous collisions), and Larmor motion can be relevant. In collisionless space plasmas classical collisions can be neglected, and velocity randomization is provided by wave-particle interactions and Larmor motion.

There are two practical ways to derive the MHD equations: Either by taking velocity moments of the Boltzmann equation, or by assuming that the plasma is magnetized gas with the electromagnetic forces added. In the latter framework, the continuity equation of fluid mechanics (e.g., Landau and Lifshitz, 1959) is

$$\frac{\partial \rho}{\partial t} + \nabla \cdot (\rho \mathbf{v}) = 0, \tag{3.1}$$

where $\rho = nm$ is the mass density, $m = m_i + m_e$ the mass, and $\mathbf{v} = (m_i \mathbf{v}_i + m_e \mathbf{v}_e)/m$ the bulk velocity of the plasma; ion and electron fluids are denoted by the subscripts i and e. Eq. (3.1) implies mass conservation, and holds in MHD as it is. In fluid mechanics, the Euler equation (Landau and Lifshitz, 1959), or the momentum equation, is given by

$$\rho \frac{d\mathbf{v}}{dt} = \rho \left(\frac{\partial \mathbf{v}}{\partial t} + \mathbf{v} \cdot \nabla \mathbf{v} \right) = -\nabla P, \tag{3.2}$$

where $P = P_i + P_e$ is the plasma pressure. Eq. (3.2) is the equation of motion for charge-neutral fluids; to apply it for plasmas the electromagnetic force density for a plasma fluid element need to be accounted for. In electrodynamics, the force on a charged particle is given by the Lorentz force $q\mathbf{v} \times \mathbf{B}$, where q is charge of the particle, and $\mathbf{B}$ is the magnetic field. The Lorentz force density for a plasma fluid element is obtained by summing over n particles in the fluid element, and is given by $\mathbf{j} \times \mathbf{B}$, where $\mathbf{j} = nq\mathbf{v}$ is the current density. Hence the momentum equation in MHD for a case with only electromagnetic forces can be written as

$$\rho\frac{d\mathbf{v}}{dt} = \rho\left(\frac{\partial \mathbf{v}}{\partial t} + \mathbf{v}\cdot\nabla\mathbf{v}\right) = -\nabla P + \mathbf{j}\times\mathbf{B}. \tag{3.3}$$

In fluid dynamics the energy equation is written as

$$\frac{d}{dt}(P\rho^{-\gamma}) = 0 \Leftrightarrow \frac{dP}{dt} = -\gamma P\nabla\cdot\mathbf{v}, \tag{3.4}$$

where γ is the adiabatic constant. This equation also applies to MHD as it is.

The relation between the current and electric field, the *generalized* Ohm's law, can be derived by subtracting the ion and electron momentum equations (assuming quasineutrality as well as neglecting the electron - ion mass ratio: $m_e/m_i \sim 0$)

$$\mathbf{E} + \mathbf{v}\times\mathbf{B} = \frac{\mathbf{j}}{\sigma} + \frac{1}{ne}(\mathbf{j}\times\mathbf{B} - \nabla\cdot\mathbf{P}_e) + \frac{m_e}{ne^2}\left[\frac{\partial \mathbf{j}}{\partial t} + \nabla\cdot(\mathbf{jv} + \mathbf{vj})\right], \tag{3.5}$$

where $\mathbf{P}_e$ is the anisotropic electron pressure tensor. In the ideal MHD conductivity is assumed infinite, and therefore $\mathbf{j}/\sigma \to 0$. Ideal MHD further assumes that the right hand side of Eq. (3.5) is small, and that the Ohm's law becomes $\mathbf{E} + \mathbf{v}\times\mathbf{B} = 0$. In the MHD description of solar wind - magnetosphere interaction the spatial scale of interest is typically a few thousand kilometers. In this scale, the $\nabla\cdot\mathbf{P}_e$ -term is unimportant because the electron pressure transverse to the direction of the magnetic field vary significantly over typically tens of kilometers, because it is proportional the spatial scales of the order of the ion inertial length $\lambda_i = c/\omega_{pi}$, where c is the speed of light and ω_{pi} is the ion plasma frequency. Furthermore, the last term in the right hand side is significant only in the very short spatial scales, because it is proportional to the electron inertial length ($\lambda_e = c/\omega_{ei}$, a few kilometers typically in space plasmas). However, the $\mathbf{j}\times\mathbf{B}$ term, the Hall term, becomes important especially in current sheets, such as at the magnetopause and in the magnetotail. Therefore, the ideal MHD assumption is valid in typical problems involving the solar wind and magnetosphere, with the exception of the thin current sheets, where the Hall term is large.

MHD equations also need an evolution equation for the magnetic field, which is obtained from Faraday's law. Using Ohm's law for ideal MHD, Faraday's law becomes

$$\frac{\partial \mathbf{B}}{\partial t} = -\nabla\times\mathbf{E} = \nabla\times(\mathbf{v}\times\mathbf{B}), \tag{3.6}$$

which is also known as the convection equation (the first term in induction equation in Section 1.2.1). Furthermore, in MHD the Ampère's law is used to define the current density:

$$\mathbf{j} \equiv \frac{1}{\mu_0}\nabla\times\mathbf{B}, \tag{3.7}$$

where the displacement current is neglected. Equations (3.1), (3.3), (3.4), and (3.6) define a closed set of equations for ideal MHD.

There are three wave modes in ideal MHD: slow magnetosonic, Alfvén, and fast magnetosonic waves, in the order of their propagation velocities. The Alfvén wave propagates perturbations transverse to the magnetic field, and moves fastest along the magnetic field. The slow and fast magnetosonic waves are compressional waves that

require plasma compression to propagate (e.g., the bow shock is a steepened fast mode wave). As MHD treats the plasma as a fluid, it does not reproduce any of the properties of the individual charged particles, such as gyration around the field line. The individual particle properties need to be handled using the plasma kinetic theory.

3.2 Numerical solutions of MHD description

Computers have enabled a new possibility to describe the Earth's plasma environment using numerical simulations. As the near-Earth plasma system includes both microphysical and macrophysical properties, an accurate numerical simulation should use a theory that can reproduce both small and large scale plasma physics phenomena. On the other hand, a numerical simulation should also be computationally efficient. A global simulation of the entire solar wind - magnetosphere system based on the kinetic theory is still beyond the capabilities of even the fastest computers, and therefore the MHD theory provides a sufficiently suitable compromise to the numerical solution of the solar wind - magnetospheric processes. As long as the scientific problem at hand deals with adequately large scales (e.g., 0.5 R_E), the ideal MHD theory is largely applicable in the near-Earth space. In particular, the solar wind, the magnetosheath, the outer tail including the lobes and the plasma sheet are well described by the MHD simulations. The inner magnetosphere is problematic, because the overlapping different plasma populations with vastly different temperatures cannot be adequately modeled with a single temperature MHD equations. Thin boundaries (such as the magnetopause) where particle kinetic properties become important, can pose a problem. However, later it is shown that the used MHD code, GUMICS-4 (Grand Unified Magnetosphere Ionosphere Coupling Simulation), reproduces well also the magnetopause location.

There are many advantages in using the global MHD simulations. First, they can describe the self-consistent dynamic evolution of the entire system based on upstream solar wind and IMF measurements only, providing an invaluable opportunity to e.g. space weather forecasting. Second, they can be applied to the entire system in a computationally efficient manner, as powerful numerical methods are available for solving the MHD equations in a discrete grid. Third, they can provide an instantaneous picture of the entire system, and thus they can provide a global setting for a more detailed examination, which can be complemented by observations made by Earth-orbiting spacecraft. Fourth, in many cases detailed measurements of the system can be difficult or impossible (e.g., in the plasma environment of distant galaxies), in which case the global MHD simulations can be used instead of measurements. While there are a number of ways to build a functioning global MHD simulation, the following describes the method that is used in GUMICS-4.

As the ideal MHD system conserves mass, momentum and energy, the ideal MHD equations can be written in conservative form, where a conserved quantity in a closed volume changes only if there is a flux of the conserved quantity through the boundaries of the volume:

$$\frac{\partial u_a}{\partial t} + (\nabla \cdot \mathbf{F}_a) = 0 \tag{3.8}$$

where u_a is the conserved quantity and $\mathbf{F}_a(u)$ is the flux function corresponding to u_a. The subscript $a = 1 \ldots 8$ corresponds to the conserved variables $(\rho, \mathbf{p} = \rho\mathbf{v}, U, \mathbf{B})$, and the corresponding equations in the conservative form are

$$\frac{\partial \rho}{\partial t} = -\nabla \cdot (\rho \mathbf{v}), \tag{3.9}$$

$$\frac{\partial \mathbf{p}}{\partial t} = -\nabla \cdot \left(\frac{\mathbf{pp}}{\rho} + P + \frac{B^2}{2\mu_0} - \frac{1}{\mu_0}\mathbf{BB} \right), \tag{3.10}$$

$$\frac{\partial U}{\partial t} = -\nabla \cdot \left[(U + P - \frac{B^2}{2\mu_0})\frac{\mathbf{p}}{\rho} + \frac{1}{\mu_0}(\mathbf{B} \times \frac{\mathbf{p}}{\rho} \times \mathbf{B}) \right], \tag{3.11}$$

where U is the total energy density given by

$$U = \frac{P}{\gamma - 1} + \frac{1}{2}\rho\mathbf{v}^2 + \frac{\mathbf{B}^2}{2\mu_0}. \tag{3.12}$$

Eq. (3.8) indicates that the global MHD simulations are essentially numerical solutions of discretized nonlinear partial differential equations. A particularly suitable spatial discretization method for the three dimensional ideal MHD system is the finite volume method (FVM), where the simulation box is divided into grid cells. FVM deals with known cell averages

$$u_{a,j}(t) = \frac{1}{V_j} \int_{V_j} u_{a,j}(\mathbf{r}, t) dV_j, \tag{3.13}$$

where V_j is the volume of the jth cell. In the FVM method the fluxes through cell faces are added and subtracted from the cell averages, leading automatically to conservation of the conserved quantities in arbitrary (even unstructured) grids.

A global MHD simulation requires a simulation box with initial and boundary conditions. The initial boundary conditions include the dipole field in the empty space as well as the input variables introduced from the sunward boundary of the simulation box; outflow conditions are applied to other boundaries of the simulation box. The introduction of the input variables leads to a *Riemann problem*, in which a discontinuity of a conserved variable exists between two constant grid cells[1], and a solution is wanted after a time Δt. A solution to a Riemann problem in MHD consists of seven waves that propagate away from the discontinuity. Two of the waves correspond to the fast magnetosonic wave, two are Alfvén waves, and two are slow magnetosonic waves. The remaining seventh wave corresponds to the bulk velocity of the plasma and is generally called an entropy wave. Consequently, it turns out that the MHD equations written in the form of Eq. (3.8) define an eigensystem, with eight eigenvalues that correspond to the seven waves and one "null" wave, whose amplitude is zero due to $\nabla \cdot \mathbf{B} = 0$.

As the cell averages are known, the accuracy of the numerical method using FVM depends on the method with which the flux through the cell interfaces are obtained. The exact solution to the Riemann problem is difficult in MHD and as such it is also computationally expensive. Fortunately, there are a number of ways to obtain an approximate

[1]For example, a removal of a membrane from between a high- and low-density regimes of a volume is a Riemann problem.

solution to the Riemann problem. One such approximate Riemann solver is a Roe solver (e.g., LeVeque, 1992). In the Roe solver, the nonlinear Riemann problem of Eq. (3.8) is linearized in the vicinity of each cell face by assuming that $u = u^{(0)} + u^{(1)}$, where $u^{(1)}$ is a small perturbation, and expanding $\mathbf{F}(u)$ into Taylor series. Applying only the first two terms of the Taylor series in Eq. (3.8) leads to an eigenvalue problem, which returns the seven eigenvalues corresponding to the MHD wave speeds. In essence, the Roe solver therefore establishes an approximation of the different wave velocities in the vicinity of each cell face, and this approximation is used to obtain the corresponding fluxes at the cell faces. The fluxes at the cell faces are then used to update the cell averages of the neighboring cells. Methods where an estimate of the cell interface flux is used to update the cell averages of the neighboring cells are generally called Godunov-type.

The problem of the Roe solver is that it works only in one dimension (defined usually as the x-direction), and the solutions for the other two dimensions are obtained by rotations. Hence, each dimension is solved independently, which introduces a risk that $\nabla \cdot \mathbf{B}$ does not remain zero. Brackbill and Barnes (1980) introduce a convenient way to remove the divergence of $\mathbf{B}$. This is called elliptic cleaning, where first $\hat{\mathbf{B}} = \mathbf{B} + \nabla\phi$ is defined, after which it is required that $\nabla \cdot \hat{\mathbf{B}} = 0$. This leads to an elliptic Poisson equation $\nabla \cdot \mathbf{B} = -\nabla^2\phi$, which is solved and finally $\mathbf{B}$ is replaced with $\hat{\mathbf{B}}$.

A problem with the conservative form MHD equations is that the plasma pressure P is calculated from Eq. (3.12) by subtracting the kinetic and magnetic energy densities from the total energy density U. Particularly in plasmas where the magnetic pressure is large compared to the thermal pressure, ($\beta = P_{thermal}/P_{magnetic} < 1$), total pressure may become negative, because the magnetic and kinetic energy densities together are numerically nearly equal to the total energy density as the thermal energy density is small. This problem is often reduced by decomposing the magnetic field into the internal dipole field and an externally induced part, i.e., $\mathbf{B} = \mathbf{B}_0 + \mathbf{B}_1$ (Tanaka, 1994), which allows computing the pressure from the relation

$$P = (\gamma - 1)\left(U_1 - \frac{1}{2}\rho\mathbf{v}^2 - \frac{\mathbf{B}_1^2}{2\mu_0}\right), \tag{3.14}$$

where U_1 is the energy density, a conserved quantity (Tanaka, 1994) related to the externally induced part of the magnetic field $\mathbf{B}_1$. Furthermore, adding diffusion explicitly prevents sometimes the formation of negative pressures, as the numerical solution to MHD equations at sharp gradients may be unphysical due to finite spatial discretization. For the latter reason, also grid refinement at locations of sharp gradients helps in obtaining solutions that are numerically closer to the analytic solution. Despite of these precautions implemented also in GUMICS-4, the Roe solver can sometimes produce negative pressures or densities corresponding to one or more of the seven eigenmodes of the Riemann problem. Namely, if there is a jump in B_x in the one-dimensional x-directed Roe solver, then $\nabla \cdot \mathbf{B} \neq 0$, which may lead to unphysical solutions of MHD equations including negative pressures. In GUMICS-4, in this situation the Roe solution at that cell interface is replaced by a Harten-Lax-van Leer (HLL) solution of the Riemann problem, where the seven intermediate states corresponding to seven MHD waves are replaced by one average of the left and right states, and as an average it is also always positive if the neighboring states are positive (Janhunen, 2000). Janhunen

(2000) proved that the positivity of the neighboring states is guaranteed also in the case of a jump in B_x if one adds a source term relative to $\nabla \cdot \mathbf{B}$ to the Faraday's law. In practice, the Roe solver works in almost all of the hundreds of thousands of cells in GUMICS-4, and the HLL method is needed typically only in less than 1% of the cell interfaces.

It is possible to define an order of the numerical method by defining the difference between the exact and computed solutions. The method used in GUMICS-4 is first order accurate both spatially and temporally. A usual problem of first order schemes is that they give smeared solutions at local discontinuities due to numerical diffusion. As any numerical method calculates the cell average using the cell averages of the neighboring cells, near discontinuities there always exists numerical diffusion due to nearby cells. A more refined grid resolution usually diminishes the numerical diffusion. However, in Godunov-type methods there is no smearing unless the discontinuities are moving. Furthermore, the solution at discontinuities in the first order method used in GUMICS-4 is one of the sharpest among the first order schemes in general (LeVeque, 1992). On the other hand, a usual problem of the second order schemes is that while the solution is sharper at the discontinuity, the solution oscillates near the discontinuities, and may even lead to negative densities or pressures. This may be even a worse problem than smeared discontinuities in some cases, since the erroneous oscillation of the solution may lead to erroneous physical interpretations.

3.2.1 GUMICS-4 MHD simulation

GUMICS-4 (Janhunen, 1996) is a global MHD simulation, which solves the MHD equations in the conservative form of Eq. (3.8) in the solar wind and in the magnetosphere. The MHD simulation box in the X direction reaches from 32 R_E to -224 R_E, the Y and Z directions reach ± 64 R_E. In the near-Earth region the MHD simulation box is limited by a 3.7 R_E spherical shell, which maps along the dipole field to approximately 60° in magnetic latitude. The grid in the MHD simulation box is a Cartesian octogrid, and it is semi-automatically adaptive indicating that whenever the code detects spatial gradients, the grid is refined. The grid refinement is called semi-automatic because the refinement depends on location, such that in the near Earth region the grid is more easily refined than further away from the Earth, where one wants to avoid too accurate calculation and save computation time. Furthermore, the code uses subcycling (variable time step) to save computation time (Janhunen et al., 1996). The time step varies with the local travel time of a fast magnetosonic wave across a grid cell, and thus it obeys the Courant-Friedrichs-Lewy condition[2]. The largest time step has been set to 1 s. Solar wind input variables (T, ρ, $\mathbf{v}$, $\mathbf{B}$) are treated as boundary conditions in the sunward wall of the simulation box; outflow conditions are applied on other walls of the simulation box. A dipole is placed in the origin. Initially, a mirror dipole sunward of the Earth's dipole is implemented to obtain a "seed" magnetopause, however, it does not affect the calculation in any way.

[2]CFL condition: the time step must be smaller than the travel time at which information is transferred within the simulation grid cell.

The MHD magnetosphere is coupled to a high-resolution ionosphere. The ideal MHD equations are not applicable in the resistive ionosphere, and therefore the ionospheric domain uses electrostatic equations. The ionosphere is a spherical shell at an altitude of 110 km (from the surface of the Earth), which is mapped to the magnetosphere using dipole field lines. The region between the ionosphere and the 3.7 R_E shell is a passive medium, which only transmits electric effects, and where no currents flow perpendicular to the magnetic field. A triangular finite element grid of the ionosphere is fixed in time, although refined to ∼100 km spacing in the auroral oval region.

Figure 3.1 presents the general structure of GUMICS-4. The magnetosphere delivers the field-aligned currents $j_\parallel$ and the electron precipitation to the ionosphere. The precipitating electrons are assumed to originate from a Maxwellian distribution from the magnetosphere. The energy flux of precipitating electrons ϵ_{prec} is calculated by setting the ratio of parallel and perpendicular temperatures $T_\parallel/T_\perp = 1$ and the parallel potential drop to $V = 0$ in Eq. (12) of Janhunen and Olsson (1998), yielding

$$\epsilon_{prec} = \sqrt{\frac{2}{\pi m_e}} n_e T_e^{3/2} \tag{3.15}$$

where m_e is electron mass and electron temperature T_e is calculated from the ion temperature of the MHD fluid by assuming $T_e = T_i/5$ (a user-defined option). As the electrons precipitate into the ionosphere they collide with atmospheric particles causing ionization. Furthermore, solar UV causes ionization in the dayside ionosphere. Therefore electron precipitation and UV radiation from the Sun are treated as sources in the calculation of the ionospheric electron density n, which in turn is eventually calculated in 20 nonuniform altitude levels in the three-dimensional ionospheric grid as

$$\frac{\partial n}{\partial t} = Q(\chi\rho, T, V) - \alpha n^2, \tag{3.16}$$

where α is the recombination rate and $Q(\chi\rho, T, V)$, which depends on the used atmospheric model, is a precomputed function of the loss cone filling rate $\chi \in [0, 1]$, source plasma mass density ρ and temperature T, and the parallel potential drop V, which is assumed zero (Janhunen, 1996).

The ionospheric electron density is used in the calculation of the local height-integrated Pedersen and Hall conductivities (Σ_P and Σ_H, respectively)

$$\Sigma_{P,H} = \int dh F_{P,H}(z) n \tag{3.17}$$

where $F_{P,H}(z)$ are coefficients for the Pedersen and Hall conductivities, respectively, and depend only on the ionospheric height profile of the atmospheric model (Janhunen and Huuskonen, 1993). The horizontal current distribution in the ionosphere is calculated from the height-integrated Pedersen and Hall conductivities and the field-aligned current distribution $j_\parallel$ is determined from the ionospheric height-integrated Ohm's law and ionospheric current continuity (e.g., Boström, 1974)

$$\mathbf{I}_\perp = \Sigma_P \mathbf{E} + \Sigma_H \hat{\mathbf{b}} \times \mathbf{E}, \tag{3.18}$$

$$j_\parallel = -\nabla \cdot \mathbf{I}_\perp \tag{3.19}$$

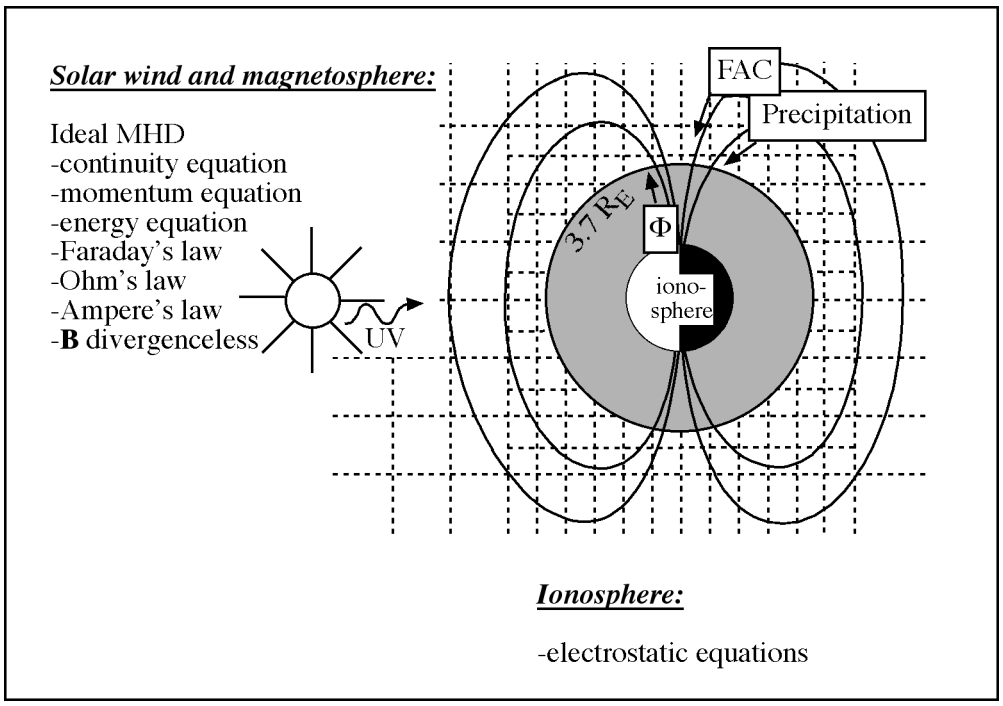

Figure 3.1. The structure of GUMICS-4 (not to scale).

where $\mathbf{I}_\perp$ is the ionospheric height-integrated horizontal current density, $\mathbf{E}$ is the ionospheric electric field, and $\hat{\mathbf{b}}$ is the magnetic field unit vector. Together Eqs. (3.18) and (3.19) yield

$$\Sigma_P \nabla^2 \Phi + \nabla \Sigma_P \cdot \nabla \Phi - \hat{\mathbf{b}} \cdot \nabla \Sigma_H \times \nabla \Phi = j_\parallel \tag{3.20}$$

which is an elliptic boundary value problem for the ionospheric potential Φ (Janhunen and Huuskonen, 1993). Once the ionospheric potential is known, it is mapped back to the 3.7 R_E shell, where $\mathbf{E} \times \mathbf{B}$ is computed and used as a boundary condition for the MHD equations. The ionospheric feed-back loop is calculated once in every four seconds.

Figure 3.2a shows the plasma density color-coded in the GUMICS-4 simulation. The bow shock, the magnetosheath, and the magnetopause are clearly visible, as are the tenuous tail lobes and the denser plasma sheet. Figure 3.2b shows the ionospheric Hall conductivity at the same instant of time. The dayside conductivity enhancement due to solar UV is visible along with the auroral oval, with a maximum conductivity enhancement on the nightside due to the magnetospheric electron precipitation.

3.2.2 GUMICS-4 relative to other global MHD simulations

Currently, there are less than ten functioning global MHD codes in the world designed specifically to solve the solar wind - magnetosphere - ionosphere system. Of these, GUMICS-4 is the only one in Europe. Studies similar to those presented in this thesis

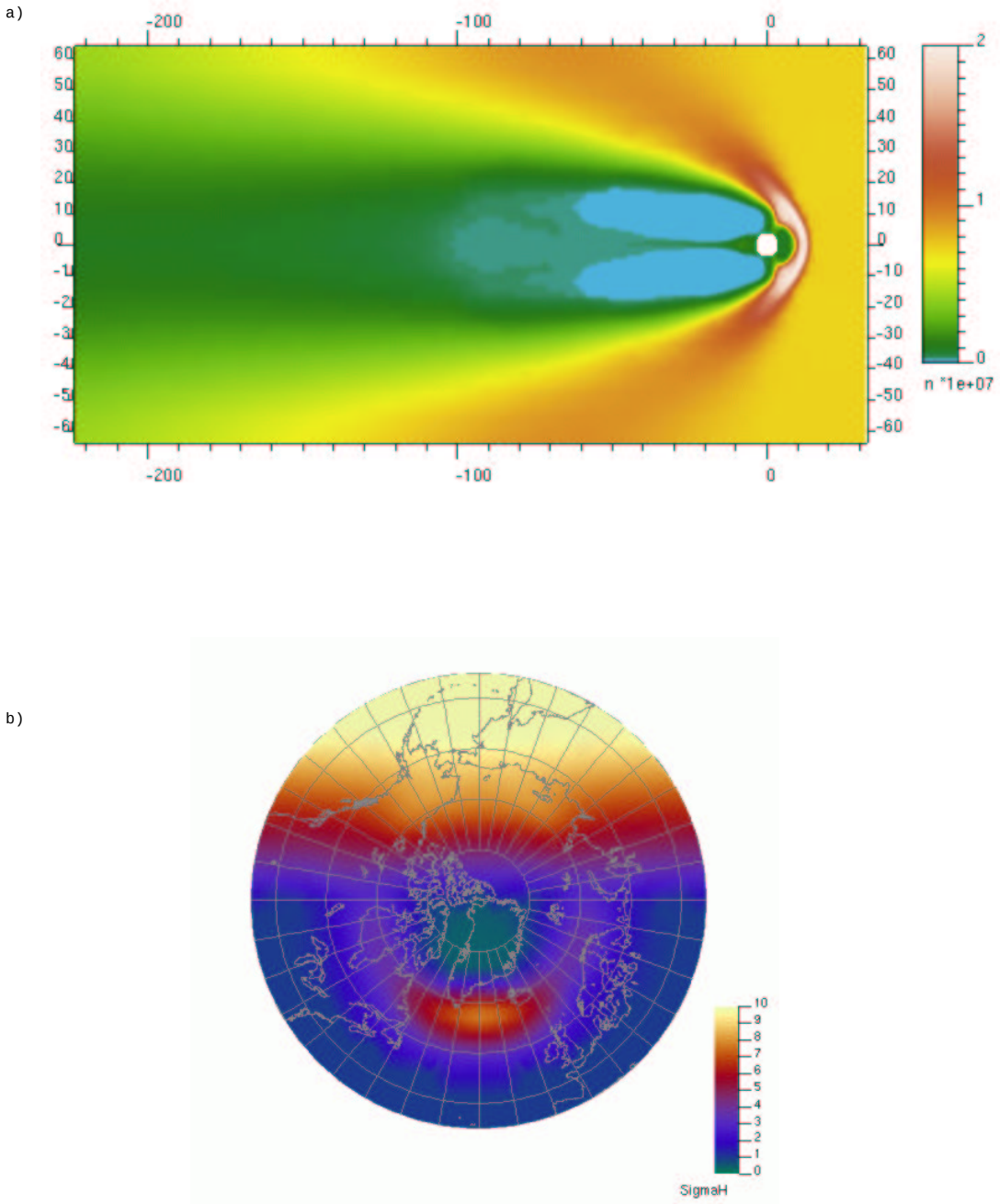

Figure 3.2. a) The density color-coded in the GUMICS-4 global MHD simulation box at the noon-midnight meridian. b) The ionospheric Hall conductivity in the Northern Hemisphere in the GUMICS-4 simulation.

have been carried out with e.g., Lyon-Fedder-Mobarry code (LFM, Fedder et al., 1995a; Fedder and Lyon, 1995; Mobarry et al., 1996), the BAT-R-US code (Powell et al., 1999), and the Geospace General Circulation Model (GGCM, e.g., Raeder et al., 1995). While the implementation of different codes vary to some extent, in general the solar wind and the magnetosphere are described with ideal MHD equations, and the ionosphere is in most cases electrostatic solving the potential distribution in the ionosphere, which couples to the magnetosphere via field-aligned currents. In the outer magnetosphere, the dynamics are often reproduced quite reliably, as verified by comparisons with *in situ* spacecraft measurements, while the inner magnetosphere still poses problems, because the overlapping ring current and plasmasphere plasmas cannot be correctly represented by the single-fluid MHD description (e.g., Pulkkinen et al., 1998).

While the current global MHD codes use different computational schemes for solving the MHD equations, the results in the magnetosphere (MHD domain) are often quite similar. Typically the boundary conditions as well as the grid implementation vary; for example, most of the global MHD codes limit their inner boundary of the MHD domain to 2-4 R_E distance in order to save computation time. In GUMICS-4, the computational efficiency is further improved in the MHD domain as the code uses subcycling, which is currently not used in other global MHD simulations of the solar wind - magnetosphere - ionosphere system. Furthermore, most of the current MHD simulations use fixed grids in the MHD simulation box, although the grids are typically refined in the near Earth region (e.g., Fedder et al., 1995a). Powell et al. (1999) introduce a code with an adaptive grid; however, the adaptation is implemented in blocks rather than cell-by-cell as in GUMICS-4.

The implementation of the ionosphere in GUMICS-4 is different from other codes currently in use. Differences appear for example in the calculation of the ionospheric conductivity, which is not typically computed in the manner presented above. Instead, the conductivity due to precipitation is typically assumed to originate from a "diffuse" and "accelerated" sources of precipitation (e.g., Fedder et al., 1995b; Raeder et al., 1998). The "diffuse" precipitation is typically calculated by making assumptions on the precipitation electron flux and characteristic energy, after which the height-integrated Pedersen and Hall conductivities are calculated using e.g., empirical formulation of Robinson et al. (1987). The "accelerated" precipitation source is due to a parallel potential drop in regions of upward field-aligned currents. As the the ionospheric grid is in any case too coarse to capture the discrete arcs (scale sizes typically of tens of kilometers) GUMICS-4 sets the parallel potential drop to zero and does not attempt to include discrete arc physics. GUMICS-4 reproduces typical values for ionospheric conductivities as compared to e.g., Kamide and Baumjohann (1993). However, the GUMICS-4 polar cap potential difference is typically a few tens of percents lower than what is observed. In contrast, other global MHD simulation codes typically give polar cap potential differences about twice the observational value (e.g., Slinker et al., 1999).

3.3 Cusp and magnetopause in MHD

Paper III investigates the cusp and magnetopause locations in the GUMICS-4 simulation. Although the MHD description does not include the characteristic charged particle processes within the cusp, a global simulation can be used to monitor the cusp at all times at all locations, allowing for parametrization of the cusp behavior as a response to solar wind and IMF variations. Furthermore, in the simulation the cusp response to one solar wind parameter can be investigated while keeping the other parameters constant. If the code performance pertinent to the cusp is verified, the cusp properties in response to different solar wind conditions in the simulation can give important information that is observationally difficult to obtain.

Although there are no particles in MHD, the various characteristics that are used in the cusp identification from satellite observations can still be distinguished. The last closed field line giving the equatorward edge of the cusp can be found from the simulation. In the MHD simulation the cusp is a region of enhanced pressure, which indicates that there is a surrounding pressure gradient and thus current to maintain pressure balance according to the equation $\mathbf{j} \times \mathbf{B} = \nabla P$. The current results from $\mathbf{B}_1$ according to Ampère's law, and as the field is in the opposite direction to $\mathbf{B}_0$, the cusp diamagnetic effect in the MHD simulation can be perceived. The quantity which most directly corresponds to the idea of diamagnetic depression is $|\mathbf{B}| - |\mathbf{B}_0|$, that is, the amount by which the field magnitude is weakened by the presence of plasma. Paper III notes that the first-order energy density U_1 appears as a sharp maximum in the cusp region. The total energy density in MHD given by Eq. (3.12) is dominated by the dipole term $\mathbf{B}_0^2$, and therefore a quantity $\widetilde{U}$ (given by Eq. (11) of Paper III) from which the dipole energy has been subtracted gives the energy density related to the solar wind - magnetosphere interaction. Paper III identifies the cusp from five parameters: 1) ionospheric footprint of the open-closed field line boundary (OC-boundary), 2) $|\mathbf{B}| - |\mathbf{B}_0|$, 3) $|\mathbf{B}_1| = |\mathbf{B} - \mathbf{B}_0|$, 4) U_1, and 5) $\widetilde{U}$. Items 2-5 were collectively termed as plasma proxies of the cusp, and they represent the high-altitude cusp because they were determined as locations of the variable maxima at a spherical 7 R_E shell. In contrast, the OC-boundary represents the low-altitude cusp. In Paper III the cusp location was investigated as a function of the IMF B_z and the solar wind ram pressure p_d. Therefore, four synthetic events were run, two with variable IMF B_z with small and large p_d and two with variable p_d with positive and negative IMF B_z.

Due to its relatively simple identification from both observations and global simulations, the magnetopause location and shape has been noted in several simulation studies (e.g., Ogino, 1986; Fedder et al., 1995a). However, quantitative and systematic investigations of the magnetopause position in MHD simulations and its dependence on the solar wind are still rare. Although both cusp and magnetopause positions are widely studied observationally, and many empirical models exist to forecast the magnetopause position (e.g., Shue et al., 1998), it is relevant to study the magnetopause position systematically from the global MHD simulation, e.g., for code verification purposes. Because observationally the subsolar magnetopause position depends both on the IMF B_z and p_d (Shue et al., 1998), the four synthetic events carried out with the intention to study the cusp location as a function of the solar wind parameters were

also used to investigate the subsolar magnetopause position. The magnetopause was identified using two methods: 1) the OC-boundary, which is the subsolar extent of the same field line mapped to the ionosphere and used as the cusp OC-boundary, and 2) the maximum of the duskward magnetopause currents (j_y) along the Sun-Earth line. The magnetopause location inferred from these two parameters were also compared to an empirical model by Shue et al. (1998).

3.3.1 Code verification

The cusp equatorward edge from the data set in Paper I was compared to the OC-boundary obtained from GUMICS-4. Figure 7 of Paper III shows that during southward IMF the observations are in quantitative agreement with the OC-boundary obtained from GUMICS-4: At a given southward IMF the OC-boundary from the simulation appears at the same latitude as is observed in Paper I. Furthermore, the amount (in degrees per nanotesla) by which the cusp moves equatorward as IMF B_z becomes smaller in the simulation is the same as is observed in Paper I. However, during northward IMF the Polar data set places the cusp to lower latitudes as compared to the GUMICS-4 OC-boundary, which represents the equatorward edge of the cusp in the simulation. If we assume, as it is likely, that the Polar observations of the cusp do not lie in the closed field line region, there is a discrepancy between the MHD OC boundary and the observed open-closed field line boundary during northward IMF. Furthermore, the plasma proxies appeared equatorward of the OC-boundary during northward IMF in the simulation. Paper III discusses about this problem and notes that the plasma proxies may not be a proper representation of the cusp during northward IMF. Based on the comparison to the Polar observations in Paper I, conclusions about the cusp location in the simulation can be made of events during southward IMF only.

3.3.2 Results: Cusp and subsolar magnetopause location in MHD

The four synthetic runs clearly revealed the following issues pertinent to the cusp dynamics during southward IMF:

1. The cusp shifts equatorward as the magnitude of the southward IMF increases. This result is consistent with a large number of statistical observational studies (e.g., Newell et al., 1989).

2. The high-altitude cusp shifts equatorward as the solar wind ram pressure increases. This result is consistent with the observational results of Paper I.

3. The low-altitude cusp is almost stationary as function of increasing ram pressure. This result is consistent with observations (e.g., Newell and Meng, 1994).

In MHD the magnetopause location is determined from the pressure balance between the dipole field and the solar wind pressure. As in the magnetosphere the magnetic field $B \propto r^{-3}$ and in the solar wind $p_d \propto B^2$, the expected magnetopause distance

is proportional to the solar wind dynamical pressure as $p_d^{-1/6}$. In reality, the magnetopause erosion due to imbalance of tailward magnetic flux transport triggered by dayside reconnection and sunward magnetic flux transport triggered by nightside reconnection must also be considered, and therefore the empirical models also include the IMF B_z as a parameter determining the magnetopause location (e.g. Shue et al., 1998). The subsolar magnetopause position studied in Paper III reproduces both effects. The magnetopause distance varies with $p_d^{-1/6}$ during both northward and southward IMF. Furthermore, during southward IMF the magnetopause erosion is captured with the magnetopause moving earthward with increasing southward IMF in both identification methods. During northward IMF the magnetopause from j_y currents is stationary but the magnetopause from the OC-boundary is slightly moving earthward, such that the magnetopause from the OC-boundary is furthest away from the Earth around zero IMF. As mentioned above, there might be a discrepancy between the OC-boundary in the simulation and in reality during northward IMF, and therefore the earthward motion of the OC-boundary during increasingly northward IMF has to be interpreted with care. The magnetopause position from both identification methods also compares well with the empirical model of Shue et al. (1998). The results obtained from the four synthetic events regarding the subsolar magnetopause position are consistent with our previous studies (Janhunen and Palmroth, 2001; Palmroth et al., 2001), which further supports the conclusion that at least during southward IMF the dayside boundaries in the GUMICS-4 simulation are in agreement with observations.

4 Energy transfer and dissipation

Because almost all dynamical processes within the magnetosphere are ultimately driven by the solar wind energy, the energy coupling process between the solar wind and the magnetosphere has gained a substantial interest in the past few decades (e.g., Akasofu, 1981). Lacking quantitative measurements, the energy input estimates have been deduced from the practical assumption "What goes out must come in", i.e., the input estimates have been scaled using estimates of the different energy sinks within the magnetosphere and the ionosphere. These correlative studies have produced several coupling functions, e.g., vB_{south} (Burton et al., 1975), which is the duskward interplanetary electric field that has been found to be closely correlated with magnetic activity (e.g., Gonzalez and Tsurutani, 1987). One of the most widely used experimental coupling functions is the ϵ parameter (Akasofu, 1981) given by (in SI units)

$$\epsilon = \frac{4\pi}{\mu_0} v B^2 l_0^2 \sin^4(\frac{\theta}{2}), \tag{4.1}$$

where v is the solar wind bulk speed, B is interplanetary magnetic field, θ is the angle between the IMF direction projected onto the yz plane and the dipole axis (clock angle, given by $\tan\theta = B_y/B_z$), and l_0 is an empirically determined scaling factor, which usually has been taken to be 7 R_E. While deriving ϵ, Akasofu (1981) considered three channels to which the solar wind energy is distributed: The ring current (assumed to be the largest sink), the Joule heat caused by the ionospheric closure of field-aligned currents, and the energy left in the ionosphere by the collisions between the precipitating and atmospheric particles. As no reliable measurements were available, the energy deposited through these processes was estimated using the Dst and AE indices. The free parameter l_0 was then fixed so that the total value of ϵ equaled the summed energy in the three magnetospheric sinks. Akasofu (1981) defined that a substorm develops when ϵ exceeds $\sim 10^{11}$ W, and values exceeding $\sim 10^{12}$ W lead to a magnetic storm.

Global energy budget studies have decreased the relative importance of the ring current as the major energy sink (e.g., Knipp et al., 1998; Lu et al., 1998). Traditionally, the ring current particle energies are estimated from the Dessler-Parker-Sckopke equation, which relates the energy of the ring current particles to the Dst index (Dessler and Parker, 1959; Sckopke, 1966), and is given by

$$Dst = \Delta B_{RC} = -\frac{\mu_0}{2\pi} \frac{W_{RC}}{B_0 R_E^3}, \tag{4.2}$$

where W_{RC} is the total energy of the ring current particles and B_0 is the surface magnetic field at the equator. Using this formulation, Knipp et al. (1998) estimated that the ring current was the largest sink only at the start of the storm main phase, and thereafter the ring current consumed only about 20% of the total energy distributed among the ring current and the polar ionosphere. Lu et al. (1998), using the same method, estimated that on average $\sim$30% (120 GW out of 400 GW) of the total energy distributed in the ring current and the polar ionosphere is consumed by the ring current. However, relating the Dst index to the ring current energy can be problematic as the Dst index includes also other effects (such as ground induction and other magnetospheric current

systems), which should be accounted for in the analyses. The recent estimate is that about half of the Dst depression is caused by the ring current particles (Turner et al., 2001). Therefore, recently attempts have been made to estimate the ring current energy content using *in situ* measurements. Assuming a constant ring current volume and using Polar satellite particle measurements of the ring current, Pulkkinen et al. (2002) estimated that about $0.5{\cdot}10^{15}$ J, less than half of the simultaneously estimated Joule heating energy, resided in the ring current during a 3-day storm period in May 1998.

Ionospheric Joule heating, calculated as $\mathbf{j} \cdot \mathbf{E}$, is caused by ohmic heating resulting from the closure of the field-aligned currents with a component along the ionospheric electric field. The atmosphere is first felt by the heavier ions, which start to collide with the atmospheric particles and deviate from the $\mathbf{E}{\times}\mathbf{B}$ drift direction towards the direction of the ionospheric electric field pulling the randomly walking ions. This results in a net Pedersen current (in the direction of the electric field), and consequently the power consumed in the process produces Joule heat. Observationally, the energy converted to Joule heat is difficult to estimate globally, while locally it can be derived for instance using ionospheric incoherent radars (e.g., Fujii et al., 1999), which can also account for the effect of the neutral winds on the Joule heating, as $\mathbf{j} \cdot \mathbf{E} = \mathbf{j} \cdot \mathbf{E}' - \mathbf{j} \cdot (\mathbf{U} \times \mathbf{B})$, where $\mathbf{E}' = \mathbf{E}{+}\mathbf{U}{\times}\mathbf{B}$, and $\mathbf{U}$ is the neutral wind field. Assuming that the contribution from the neutral winds is small, the Joule heating becomes $\sigma_P \mathbf{E}^2$. Therefore, estimates of global Pedersen conductivity maps based on satellite measurements (e.g., Spiro et al., 1982) or combined radar and ground magnetic field measurements (e.g., Ahn et al., 1983a), together with estimates of the global electric field maps can be used to estimate the global Joule heating rate. As both quantities depend on the level of magnetic activity, correlation analyses have yielded proxies for the Joule heat based on the AE index (e.g., Ahn et al., 1983b). However, the AE index-based methods are only as good as the ability of the AE index to describe the temporal and spatial variations of the Pedersen currents not only within the auroral regions but in the polar cap as well. As the AE stations are located at high latitudes, the true intensity of the auroral electrojets is not recorded, particularly during major storms when the auroral oval moves significantly equatorward. Furthermore, the Joule heating can be approximated using global models that use all available measurements in an assimilative way, such as the assimilative mapping of ionospheric electrodynamics (AMIE) procedure (Richmond and Kamide, 1988).

Currently it is thought that at least half of the input energy is dissipated in the polar ionosphere, both during storms (e.g., Lu et al., 1998) and substorms (e.g., Tanskanen et al., 2002). Of the ionospheric energy sinks, Joule heating is thought to dissipate more energy than the electron precipitation. Lu et al. (1998) ran a moderate storm (Dst minimum -85 nT) through the AMIE procedure (Richmond and Kamide, 1988) and concluded that on average about 50% (190 GW out of 400 GW) of the summed power distributed to the ring current and the ionosphere was consumed by the Joule heating. Knipp et al. (1998), also using the AMIE technique, estimated that roughly 60% of the summed ring current and ionospheric power was consumed by Joule heating during a prolonged storm period (Dst minimum -100 nT) lasting as long as 8 days. Note

that the above percentages are obtained by comparing to the total amount of energy of the ring current and the polar ionosphere, not relative to the input. Utilizing a large substorm data set and inferring the Joule heat using the method of Ahn et al. (1983b), Tanskanen et al. (2002) estimated that about 30% of ϵ is dissipated by the Joule heating during non-storm substorms, whereas during stormtime substorms the fraction of ϵ consumed by the Joule heating is $\sim$25%.

In contrast to the Joule heating estimates, the energy deposited in the ionosphere by the precipitating particles can be globally derived using direct measurements: Global images record light emitted by atmospheric neutrals after collisions with precipitating magnetospheric particles. Locally the precipitating particles and the associated energy flux can be measured directly by low-altitude satellites. However, based on global images from the Polar spacecraft, Østgaard et al. (2001) introduced a method to derive the global energy deposition maps caused by electron precipitation over a wide energy range. To generalize the result, Østgaard et al. (2002) correlated the energy deposited by the precipitating electrons with the AL and AE indices. However, as already noted, the AE-based proxies are capable of giving the energy deposition estimates only in the regime where the AE index describes the ionospheric processes sufficiently well. Problems are to be expected during major storms when the auroral processes move to lower latitudes, or during times when the ionospheric processes occur at locations of large spatial gaps between the AE stations (such as Siberia). Furthermore, also other proxies based on radar and ground magnetic field measurements giving the precipitation energy as a function of the AE index exist (e.g., Ahn et al., 1983b). Both Knipp at al. (1998) and Lu et al. (1998) concluded that on average 20% of the summed ionospheric and ring current energy is consumed by precipitating electrons.

Other than the three above listed energy sinks, energy is consumed in the magnetotail, as plasma sheet heating and the plasmoid release. Based on Geotail spacecraft measurements, Ieda et al. (1998) estimated that the plasmoid carries about $2{\cdot}10^{14}$ J from the magnetosphere back to the interplanetary space. Furthermore, Ieda et al. (1998) estimated that the total energy consumed in the magnetotail during a substorm can be 10^{15} J, a figure comparable with the Joule dissipation during a substorm (Tanskanen et al., 2002). Hence, e.g., Koskinen and Tanskanen (2002) argue that the tail effects should be included in the energy input estimates when determining the scaling factors for parameters such as ϵ.

4.1 Energy transfer in MHD

As mentioned earlier, the global MHD simulations can provide invaluable insight in problems that are either difficult or impossible to be solved observationally, within the limitations of the ability of the MHD equations to describe physical phenomena in the near Earth space. Quantitative evaluation of the global energy input from the solar wind to the magnetosphere is a prime example of such a problem. Locally, the energy transfer rates can perhaps be inferred using satellite observations, but it is not straightforward to generalize a local result to hold on the entire magnetopause as the conditions can change considerably over the large region involved. Furthermore, considering that

reconnection is the dominant energy transfer mechanism, the energy input through the magnetopause is a strong function of location. For these reasons, in Paper IV the GUMICS-4 global MHD simulation is used to estimate quantitatively the global energy input to the magnetosphere. Furthermore, Paper IV addresses the question of where the energy transfer takes place at the magnetopause surface.

Several steps are required to compute the total energy input to the magnetosphere in the simulation: First, a definition of the magnetopause is needed to determine the coordinates of the magnetopause location. Second, the local orientation of the magnetopause has to be determined; this is accomplished by defining the normal (unit) vector $\hat{\mathbf{n}}$ for each of the magnetopause surface elements defined by the surface coordinates. Third, the total energy flux $\mathbf{K}$, defined by

$$\mathbf{K} = \left(U + P - \frac{B^2}{2\mu_0}\right)\mathbf{v} + \frac{1}{\mu_0}\mathbf{E} \times \mathbf{B}, \tag{4.3}$$

needs to be evaluated from the simulation results in the center of each surface element. Taking the dot product of the simulation total energy flux and the normal (unit) vector of the surface element gives the component of the energy flux perpendicular to the surface element. Finally, when the perpendicular energy flux is multiplied by the area of the surface element dA, one gets the total energy that has penetrated the surface element, namely

$$dE_{element} = dA\mathbf{K} \cdot \hat{\mathbf{n}}. \tag{4.4}$$

By integrating over the surface elements, the net power E_s through the surface is calculated as

$$E_s = \int dE_{element}. \tag{4.5}$$

The most critical feature of the energy input calculation in this method is the determination of the magnetopause location. Overall, GUMICS-4 results have shown that the magnetopause position is well-determined (Janhunen and Palmroth, 2001; Palmroth et al., 2001). While Paper III identifies the magnetopause from the j_y current maximum and the OC boundary, a different approach is used in Paper IV, where the magnetopause is determined from the boundary of the void of solar wind streamlines which is formed when the streamlines bend around the magnetosphere. Methods using spatial derivatives (e.g., the location of the density gradient) were not used because they are strongly dependent on the grid resolution, which is severely decreased in the distant tail region making the boundary determinations ambiguous. The flow line mapping, which is a method using an integrated variable, is not so dependent on the grid resolution and therefore it yields a sufficiently smooth surface also in the distant tail region; this was clearly demonstrated when the different methods were tested.

4.1.1 Code verification

The 6 April 2000 storm event, described in Paper II, was simulated with the GUMICS-4 code (see animation 1 in Appendix CD). To verify the code performance, the 6 April

2000 storm simulation results were compared with *in situ* satellite measurements, as shown in Figures 2 and 3 of Paper IV. At Geotail orbit in the magnetosheath the GUMICS-4 results reproduced the magnetic field variations quite reliably both in large and small scales, although differences with *in situ* measurements were also noted. A possible reason for the differences was the constant dipole tilt of the simulation, which affects the alignment of the magnetosphere and therefore can place the Geotail orbit in the solar wind in the simulation (see animation 2 in Appendix CD), while in reality Geotail did not leave the magnetosheath during the CME sheath passage. At the GOES-8 geosynchronous orbit, the large scale variation of the magnetic field was quite well reproduced, considering that the global MHD simulations in general have problems in modeling the overlapping different plasma populations in the inner magnetosphere (e.g., Pulkkinen and Wiltberger, 2000). Furthermore, also the small-scale variations of the B_z component in the simulation was shown to correspond to observations. As the energy input calculation is most critically dependent on the magnetopause location, it was specifically noted in Paper IV that the short magnetosheath encounter of GOES-8 was captured within one grid spacing (see animation 3 in the Appendix CD). Furthermore, as Figure 4 of Paper IV shows, the subsolar magnetopause location was consistent with the empirical model of Shue et al. (1998).

4.1.2 Results: Total energy through the magnetopause in MHD

Examples of the magnetopause surfaces identified with the method described in more detail in Paper IV can be found from the Appendix CD. Figure 4.1a shows the net energy through the surface as a time series. The error bars in Figure 4.1a are obtained by calculating the net energy through a 5% larger and smaller surface and thus they account for errors related to the magnetopause location determination. 5% was taken to represent the error fluctuation, because it is close to the smallest grid size with respect to the subsolar magnetopause distance in this simulation run. Furthermore, a larger percentage was not used to avoid the risk of placing the surface inside the 3.7 R_E shell at the dayside, where the magnetopause is significantly compressed for the most part of the storm simulation. Major part of the total transferred energy was in the form of Poynting flux. As noted in Paper IV, the energy input through the magnetopause increases rapidly after the SSC (cf. Figure 1 of Paper IV) and stays enhanced during the main phase of the storm when the IMF is southward; after the northward turning of the IMF the energy input starts to decrease. Comparing with Figure 7 of Paper IV, the time series of the total energy through the surface is surprisingly similar to the ϵ parameter. However, also differences appear, particularly at the time of the SSC. These differences are most probably due to the solar wind pressure that also affects the energy input (Scurry and Russell, 1991), a parameter that is highly enhanced during this event (Paper II), and is present in ϵ only through the solar wind bulk speed. Figure 4.1b shows the net energies through the 5% larger and smaller surfaces relative to the net energy through the obtained surface (red curve in 4.1a). Figure 4.1b indicates that the relative error of the 5% larger and smaller surfaces compared to the net input energy is small during the storm main phase, whereas fluctuations of the relative error appear at the

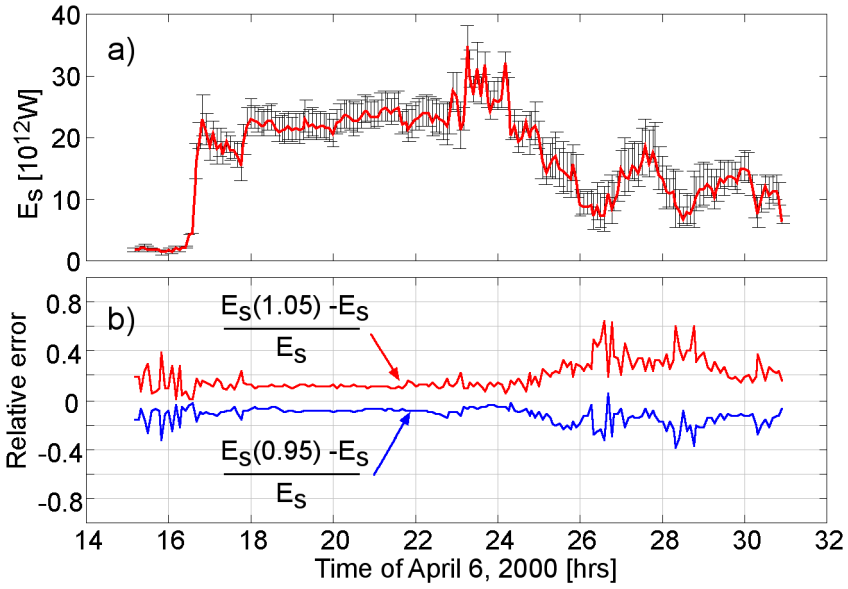

Figure 4.1. a) Total energy through the magnetopause surface in the GUMICS-4 simulation calculated using Eq. (4.5). Error bars correspond to total energies calculated on 5% larger and smaller surfaces using the same technique. b) Difference of the net energy calculated on the 5% larger (red) and smaller (blue) surfaces relative to the net energy on the obtained surface (red curve in Figure 4.1a).

SSC (around 16 UT) and during the recovery phase (00-07 UT on April 7, 2000). The fluctuations of the relative error are most probably due to the surface motion: Owing to the continuous forcing of the solar wind during the main phase the surface is more stationary than during the recovery phase, during which the surface is more mobile (cf. animation 4 in Appendix CD). However, as the relative error of the main phase energy input is at most under 10%, the energy input calculation from the simulation is argued to be sufficiently reliable.

It is quite surprising that the time variation of power E_s and ϵ is so similar, because as an instantaneous function of point measurements of the solar wind and IMF parameters, the time variation of ϵ does not necessarily have anything to do with E_s which is a measure of the total energy transferred through the magnetopause in time. Naturally, E_s is larger than ϵ, because it includes also the energy that goes through the system, while ϵ was scaled to the energy dissipated in the inner magnetosphere and ionosphere. Due to its functional form, ϵ has been related to the upstream Poynting flux, although in this case only the perpendicular component of the magnetic field should be used in equation (4.1). However, the solar wind itself carries very little energy with the Poynting flux as compared to the energy carried by the bulk flow. On the other hand, in the magnetosheath the bulk flow energy is almost tangential to the magnetopause, and therefore is not likely to enter into the magnetosphere. Furthermore, in the magnetosheath the magnetic field is compressed and the solar wind speed is decelerated, and therefore $\mathbf{v}$ and $\mathbf{B}$ are not the same as the solar wind parameters used in the calculation

of ϵ. Therefore, as pointed out by Koskinen and Tanskanen (2002), it seems a lucky coincidence that the ϵ parameter, calculated from the solar wind parameters and resembling the Poynting flux, predicts the magnetospheric energy output so efficiently (e.g., Lu et al., 1998). As ϵ and E_s are so similar, it seems evident that the Poynting flux is the controlling factor of the energy transfer into the magnetosphere, as originally put forth by Akasofu (1981). However, the reason for this is that the solar wind Poynting flux focuses toward the magnetosphere (Walker et al., 1993; Papadopoulos et al., 1999).

4.1.3 Energy transfer locations in MHD

The method of calculating the net energy through the magnetopause in MHD allows further the investigation of where on the magnetopause surface the energy transfer takes place and how does the location of energy transfer depend on the ambient solar wind parameters. Paper IV divides the magnetopause surface into four sections to investigate the energy transfer distribution along the tail, and further into six sectors to investigate the azimuthal energy transfer distribution. Paper IV revealed that the bulk of the energy input occurs on the surface earthward of -10R_E, which is natural when considering that the energy transfer may take place everywhere on the open field line between the dayside and nightside reconnection regions. Furthermore, Paper IV revealed that the energy transfer is concentrated into those sectors that are aligned with the IMF direction projected onto the yz plane. Figure 4.2 illustrates the azimuthal energy transfer during the different phases of the storm: Each diagram is an average of the azimuthal energy transfer during each phase of the storm, and the size of the colored area in each sector is proportional to the energy transfer in that sector, such that all sectors are normalized to 7000 GW (the outermost circle). The tip of the red arrow gives the average clock angle direction, the red arrow itself gives the IMF direction projected to the yz plane. Figure 9 of Paper IV shows that during the SSC and the main phase the clock angle was not fluctuating and hence it remained predominantly in one sector, but during the recovery phase the clock angle fluctuated between two sectors (240°-360°). Therefore the average of the clock angle is a good indicator of the IMF direction projected onto the yz plane only during the SSC and main phases. From Figure 4.2 it is clear that the IMF direction projected onto the yz plane determines the energy transfer sectors: Paper IV suggested that this is due to the Poynting flux focusing in the direction of the IMF (e.g., Papadopoulos et al., 1999). If no focusing of the solar wind energy transfer would occur, the sectors would show an even amount of transferred energy. The recovery phase energy transfer is problematic: Although the average clock angle is directed into the sectors where also most of the energy transfer takes place, the fluctuation of the clock angle was strong during the storm recovery. Therefore, the Poynting flux focusing may not play a major role in the energy transfer during northward IMF, and consequently Paper IV suggests that reconnection site location may have a stronger effect on the azimuthal distribution of the energy transfer during northward IMF.

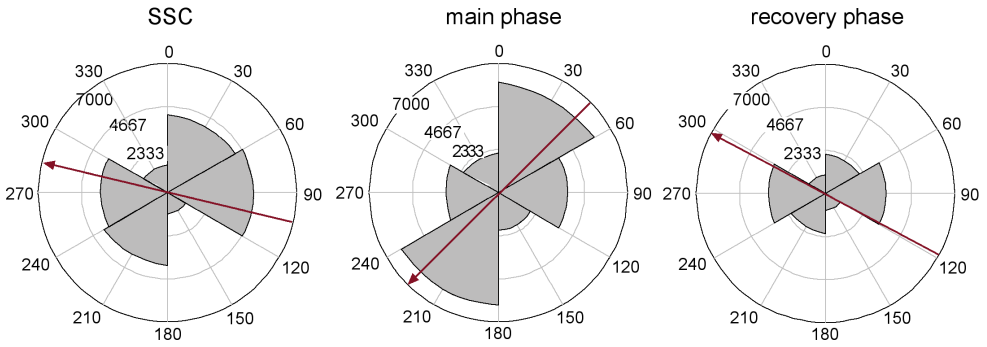

Figure 4.2. Averages of energy transfer distributed to different sectors during the SSC (1640-1700UT), main phase (1740-0030UT), and recovery phase (0030-0655UT). Sector energies are given in gigawatts and the values are normalized to 7000 GW (outermost circle). The red arrow gives the IMF direction projected onto the yz plane and the tip of the arrow gives the average clock angle during each phase.

4.2 Energy dissipation in MHD

In Paper V the scope of Paper IV is expanded further to cover the evaluation of the energy that is consumed within the ionosphere by Joule heating and electron precipitation. Simulations of two events are examined: the storm on 6 April 2000, and a substorm that occurred on 15 August, 2001. The code performance during the April 2000 storm was verified with *in situ* data comparisons in Section 4.1.1; *in situ* data comparisons verifying the code performance during the August 2001 substorm are given by Pulkkinen, T., Palmroth., M., Janhunen, P., et al., (2003, manuscript in preparation).

The height-integrated Joule heating power is calculated as

$$P_{JH} = \int \mathbf{E} \cdot \mathbf{I} dS = \int \Sigma_P E^2 dS, \tag{4.6}$$

where the integration extends over the entire surface of the ionosphere. On the other hand, the energy associated with particle precipitation is obtained using formulas given by Robinson et al. (1987), where the height-integrated ionospheric Pedersen and Hall conductivities are calculated using the energy flux and the average energy of precipitating electrons. As GUMICS-4 gives the Pedersen and Hall conductivities in the ionosphere, Eqs. (3) and (4) of Robinson et al. (1987) are analytically inverted to get the precipitation energy flux from Σ_P and Σ_H.

As Figures 3b and 6b of Paper V show, the time variation of precipitation power calculated from both events simulated by GUMICS-4 is well correlated with the empirical proxy given by Østgaard et al. (2002), but the amount of power calculated in GUMICS-4 is less than Østgaard's empirical proxy predicts. Slinker et al. (1999), who simulated a roughly similar sequence of solar wind input as compared to the 15 August 2001 substorm event, reported total precipitation powers of ∼5-25 GW, whereas our maximum integrated precipitation power for the 15 August 2001 substorm is ∼13 GW. Figure 6a of Paper V shows that in the 15 August 2001 substorm simulation the

time variation of Joule heating compares well with the empirical proxy of Ahn et al. (1983b), but the total amount of Joule heating during the substorm is much less than the empirical proxy predicts. Slinker et al. (1999) obtained total Joule heating powers of ∼125-250 GW, whereas our simulation of 15 August 2001 substorm (roughly similar input as in Slinker et al. (1999)) yielded only about 7 GW as maximum integrated Joule heating power. As mentioned earlier, the polar cap potential difference is typically 30% smaller in GUMICS-4 as compared to observations. Therefore the low value of Joule heating can be due to lower polar cap potentials in GUMICS-4.

In Figure 3a the time variation of Joule heating in the storm simulation is poorly correlated with the empirical proxy, rather it is strikingly similar with the solar wind dynamic pressure. Furthermore, also the amount of Joule heating during the storm simulation is much less than the empirical proxy predicts. Paper V hypothesizes that since the Region 1 currents that mainly cause the Joule heating in the ionosphere are connected to the Chapman-Ferraro current at the magnetopause in GUMICS-4 (Janhunen and Koskinen, 1997), they are strongly affected by the solar wind ram pressure. The closure of Region 1 currents to magnetopause currents was also noticed by Siscoe et al. (2002). Therefore events that have strong variations in the solar wind dynamic pressure have also Joule heating profiles that follow the pressure variations. Furthermore, Paper V concludes that during the storm simulation the dayside is dominating the ionospheric dissipation, whereas in the substorm simulation the ionospheric power is mainly consumed in the nightside oval.

The total amount of Joule heating in the simulation was curiously less than the total amount of precipitation power during both events, which is different from previous observational investigations (e.g., Knipp et al., 1998; Lu et al., 1998). The underestimation of Joule heating in GUMICS-4 is a consequence of several different sources, one of which is the typically 20-30% lower polar cap potentials as compared to observations. As the Joule heating is given by $\Sigma_P E^2$, underestimation of the polar cap potential by 30% leads to underestimation in the Joule heating by ∼50%. Furthermore, a small error in the GUMICS-4 total Joule heating result can also be caused by the limited ionospheric grid resolution: For example, discrete intensive arcs with sizes below the GUMICS-4 ionospheric grid resolution produce locally high values of Joule heating. Paper V estimates roughly that the discrete arcs can increase the total Joule heating up to 10%. An additional effect could be caused by a more localized field-aligned current closure: As a simplified thought experiment, let us consider a single current loop depicted in Figure 4.3 in which the magnetosphere gives the precipitation and the ionosphere is a load giving the Joule heating. This argument is rather general as any current system can be composed of a set of "wire" currents. The power P consumed in the single current loop is determined by the potential difference U and the total current I of the loop, since $P = UI$. In MHD $\nabla \cdot \mathbf{j} = 0$, and thus in a single current loop the same current flows from the magnetosphere and through the ionospheric load; $P_{msphere}/U_{msphere} = I = P_{ionosph}/U_{ionosph}$. The characteristic energy of the precipitating particles giving the upward field-aligned current determines the $P_{msphere}$, and we assume that $P_{msphere} = P_{prec}$ and $P_{ionosph} = P_{JH}$. This yields $P_{prec}/P_{JH} = U_{msphere}/U_{ionosph}$. In both simulated events $P_{prec}/P_{JH} > 1$, which means

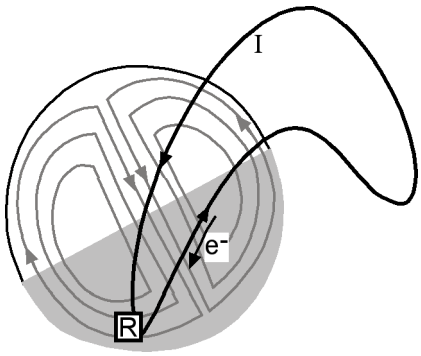

Figure 4.3. A simple current loop, where the field-aligned currents close through the ionospheric load. See text for explanation.

that $U_{msphere}/U_{ionosph} > 1$, suggesting that the current could close over a relatively short distance in the ionosphere. Satellite observations reported by Marklund et al. (1998) demonstrate that the closure of a part of the field-aligned currents in the substorm current wedge occurs locally near the surge head.

Figure 4.4 (Pulkkinen, T., Palmroth., M., Janhunen, P., et al., 2003, manuscript in preparation) shows further the various normalized energy-related properties of the 15 August 2001 substorm simulation. All the variables start to increase as the IMF turns southward, especially the polar cap area (green) defined as the area limited by the open-closed field line boundary in the simulation, indicating the activation of the energy loading process in the tail lobes. The Joule heating (red) increases in concert with the net energy through the magnetopause (black), whereas the precipitation power (magenta) and the polar cap potential (blue) start to increase slower. As IMF turns northward, all variables start to decrease, except the precipitation power which remains enhanced and decreases only later. This suggests that the Joule heating is related with the directly driven component of the substorm, whereas the precipitation power is more directly tied to the loading-unloading component of the substorm. This suggestion is supported also by noting that Figures 4 and 7 of Paper V presenting the global maps of Joule heating in the simulation show that the strongest Joule heating is produced at locations where the potential contours are closest together, suggesting that the global convection is important in the production of Joule heat.

One aim of Paper V was to examine whether a functional dependence can be found between solar wind parameters and the total ionospheric dissipation. The functional form of the power law was chosen to include the solar wind density ρ, velocity v, and the IMF B_z. The simplest power law taking these parameters into account is

$$P_{ionosphere} = C \left(\frac{\rho}{\rho_0}\right)^a \left(\frac{v}{v_0}\right)^b \left[\exp\left(\frac{B_{z,IMF}}{\sqrt{2\mu_0 p_{dyn}}}\right)\right]^d \tag{4.7}$$

where $\rho_0 = m_p \cdot 7.3 \cdot 10^6$ m^{-3} $= 1.22 \cdot 10^{-20}$ kgm^{-3} and $v_0 = 400$ km/s are chosen as typical solar wind density and velocity. With these scalings, C is a constant having units of Watts. Since the formula was chosen to be obtained by a linear multi-variable

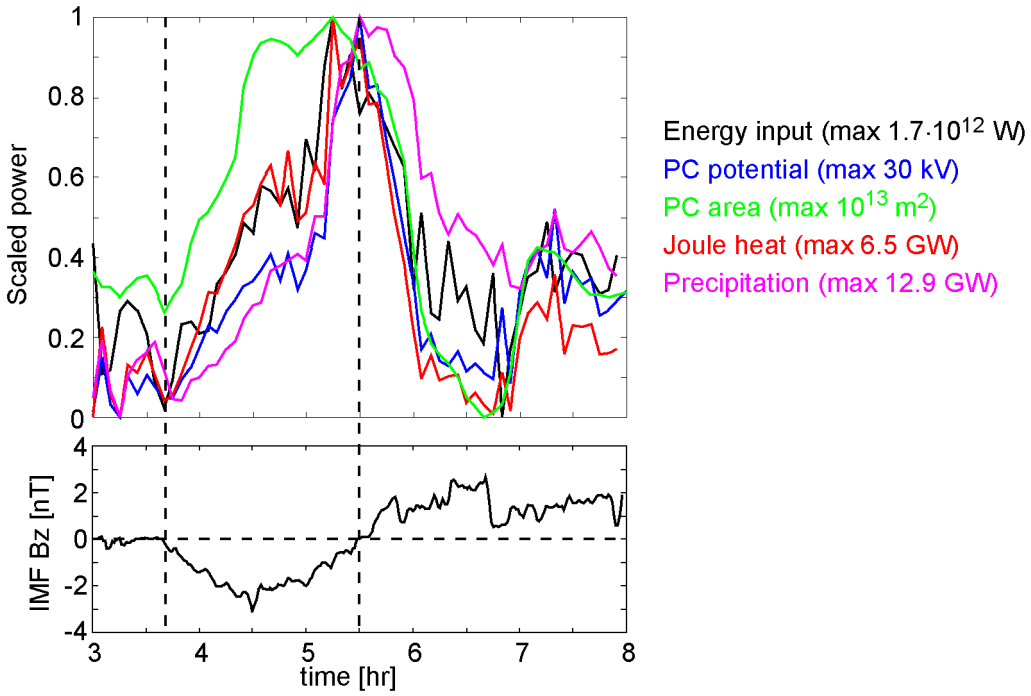

Figure 4.4. Various properties of the 15 August 2001 substorm: (black) total energy through the surface, (blue) polar cap potential, (green) polar cap area, (red) Joule heating, (magenta) precipitation power.

regression, taking a natural logarithm of both sides of the formula should yield a linear term, and therefore trigonometric functions to model the on-off property of the energy input caused by the orientation of IMF are not used, instead the IMF B_z is modeled inside an exponential. Furthermore, this is also because intuitively the left hand side of Eq. (4.7) should be positive and increase as negative IMF B_z increases. As shown by Table 3 of Paper V, at best Eq. (4.7) predicts the total ionospheric power in the simulation from the solar wind parameters with over 90% correlation for both the storm and the substorm simulations.

Fits were made for the ionospheric Joule heating and precipitation independently and for the total ionospheric dissipation given by the sum of the two terms using Eq. (4.7). Correlations with the solar wind data were shown to give highest coefficients to the total amount of ionospheric dissipation, which is natural as the two parameters are not independent of each other. The relative importance of the exponents a, b, and d suggests that the solar wind density and velocity have more impact on the total ionospheric dissipation than the IMF B_z. This may not be universally true: Coincidentally, in the two chosen events the impact of the solar wind pressure was stronger than the IMF. In the April 2000 storm the solar wind dynamic pressure was unusually high, and in the moderate August 2001 substorm the IMF B_z was quite weak and not rapidly varying. Thus, more events with different inputs must be simulated to obtain a power law that would recover the empirically found strong correlation between energy dissipation and IMF B_z.

5 Discussion and future directions

This thesis addressed the solar wind - magnetosphere coupling, particularly in light of the energy transfer and dissipation processes, both observationally and using global MHD simulations. Lacking quantitative observational methods to assess the energy coupling processes, the observational task of this thesis has been mainly to view various dynamic processes that are manifestations of the solar wind energy transfer. The solar wind control of the cusp and magnetopause locations was demonstrated. Furthermore, a major magnetic storm was described observationally. A global MHD simulation was used to quantify the energy coupling process. A method calculating the net input energy was described. Furthermore, the ionospheric dissipation was calculated from the simulation results.

Since the first three-dimensional global MHD simulations (Brecht et al. 1982; Ogino, 1986) the codes have been used in testing existing theories or developing new ones in two basic ways: Synthetic events (e.g., Raeder et al., 1995; Kullen and Janhunen, 2003), or *in situ* data comparisons (e.g., Fedder et al., 1995b; Lopez et al., 1998; Pulkkinen and Wiltberger, 2000). This has led to mainly two types of codes: Those aiming to reproduce as pure MHD as possible (such as the BATS-R-US code, Powell et al., 1999) and those that focus in reproducing the observational *in situ* data corresponding to coupled solar wind - magnetosphere - ionosphere system as correctly as possible (such as LFM code, Fedder et al., 1995a; Fedder and Lyon, 1995; Mobarry et al., 1996). Both directions have their own strengths, i.e., in the former the tractability of a certain observation to ideal MHD or in the latter the verifying the code performance in real situations in order to use the code, e.g., for space weather predictions. While GUMICS-4 belongs to the pure MHD codes, the scientific results presented in this thesis have shown that it can also be used in *in situ* data comparisons.

The studies using MHD simulations have sometimes been accused for being too qualitative in their treatment of the scientific problems. One aim of the work presented in this thesis has been to develop methods with which the simulation results can be suitably quantified. For example, using the developed methods for the automatic cusp and magnetopause identification (Paper III; Paper IV), the cusp and magnetopause locations have been shown to correspond quantitatively to observational evidence. Furthermore Paper IV shows that the developed methods can also be used in scientific problems that cannot be solved observationally. The automatic magnetopause detection method allowed for the first time the quantification of the net energy flow through the magnetopause.

Prior to Paper IV, the energy transfer process in global MHD simulations have been assessed by tracing Poynting flux lines (e.g., Walker et al., 1993; Papadopoulos et al., 1999), which has demonstrated that Poynting flux focuses through the magnetopause in the tail during southward IMF. However, the Poynting flux mapping does not specify the amount of energy transferred along these paths. Furthermore, instead of the non-conservative Poynting flux we have used a conserved quantity, the total energy flux. The total energy through the magnetopause was curiously found to resemble the temporal variation of the ϵ parameter, although it is naturally much larger than the ϵ estimating

the consumed, not transferred, energy. The same behavior was further confirmed by simulations of other events (e.g., Palmroth et al., 2002). Since the Poynting flux has been demonstrated to focus toward the magnetosphere (e.g., Papadopoulos et al., 1999), it is only natural that power E_s has the temporal variation of the Poynting flux. Therefore the efficiency of ϵ to predict the energy transfer periods is due to the Poynting flux that is focused towards the magnetopause, although the ϵ itself is calculated using solar wind parameters.

Utilizing the new methodology developed in Paper IV the energy transfer locations were identified for the first time. While the entering of the Poynting flux through the magnetopause as well as its focusing in the IMF direction projected onto the yz plane have been known (Papadopoulos et al., 1999), the actual demonstration of the energy transfer location as a function of the clock angle has not been carried out prior to Paper IV. During southward IMF the energy was evidenced to transfer mainly sunward of -10 R_E in the sectors that are aligned with the IMF direction projected onto the yz plane. This suggests an active energy focusing process, otherwise an even distribution of energy would be transferred throughout the surface. The energy transfer location dependence on the solar wind parameters was also corroborated with another event simulation (Palmroth et al., 2002). A natural explanation for the energy transfer occurring in distinct sectors is again the Poynting flux focusing. It is not clear whether the Poynting flux focusing controls the energy transfer locations also during northward IMF. Instead, the reconnection location might have a more decisive role in the energy transfer during northward IMF. However, Paper III reported cautiously that overall the northward IMF may pose a problem in the identification of the cusp and magnetopause locations. Therefore the code performance must be systematically examined during northward IMF. Future studies will also include the comparison of energy transfer during northward IMF in GUMICS-4 and in the analytic magnetosheath flow model by Kallio and Koskinen (2000).

The new methodology designed in Paper IV for detecting the magnetopause surface automatically from the simulation can, in principle, be applied to any given surface within the magnetosphere with relatively few changes in the detection routine. For instance, a suitable method for detecting the plasmasheet boundary layer will be developed in the future, and as this surface is fundamentally important in e.g., substorm studies, significant new results concerning the tail disruption process can be expected. As Paper IV warned, due to the numerical method used in GUMICS-4, the surfaces detected from the simulation can only be used in calculating surface integrals, such as the net energy through the surface. They cannot be used in the Gauss' law manner for calculating volume integrals, such as the energy contained inside the surface. However, the surface bounds a volume, and a new method for calculating volume integrals based on the surface detection has already been implemented. This method has been used in calculating e.g., the total volume, mass, and different energy components contained inside the surface. These results, as well as the application of the method to other simulated events, are likely tho give new insight to the overall energetics of the coupled solar wind - magnetosphere - ionosphere system.

Regarding the energy dissipation, two main dissipation channels in the ionosphere

are quantified in the GUMICS-4 simulation. The time variation of energy deposited to the ionosphere by precipitating electrons is shown to correlate with an empirical proxy (Østgaard et al., 2002), however the amount of energy is smaller in GUMICS-4 than is predicted by the empirical proxy. Some of the apparently lacking precipitation energy in the simulation can be accounted for the inner boundary of the MHD simulation domain, which maps to $\sim 60^\circ$ in magnetic latitude. Therefore, at least in the 6 April 2000 case, the oval boundary was equatorward of the simulation limit, and hence a portion of precipitation was not modeled. On the other hand, also the empirical proxy (Østgaard et al., 2002) gives the precipitation power using the AL index, which is calculated from magnetometer stations located poleward of the main part of the oval during the 6 April 2000 storm. Thus there are uncertainties in both the MHD result and in the empirical proxy during the storm simulation. The 15 August 2001 substorm was so small that the oval maps to the the MHD domain, however, also during this simulation the precipitation levels were small compared to the empirical proxy (Østgaard et al., 2002). At the time of the simulations were carried out the precipitation energy was not among the variables stored from the simulation, and thus it was calculated using empirical formulas of Robinson et al. (1987). Therefore, the first task in the future pertaining the precipitation is to check if the situation changes after the precipitation energy is directly computed and saved during the simulation run. Furthermore, to calibrate the GUMICS-4 results the precipitation must be compared against the observational estimate of the precipitation energy, not to an empirical proxy. Only after this can we draw final conclusions on the amount of precipitation in GUMICS-4.

The temporal variation of Joule heating calculated from GUMICS-4 was shown to correlate with an empirical proxy (Ahn et al., 1983b) only during the 15 August 2001 simulation. Instead, the temporal variation of Joule heating during the 6 April 2000 simulation resembled strikingly the temporal variation of the solar wind dynamic pressure. It was suggested that as the Region 1 currents close to the magnetopause currents, their intensity is controlled by the solar wind ram pressure, and therefore the Joule heating associated with the closing of the Region 1 currents would be also controlled by the ram pressure. Furthermore, our yet unpublished results have shown that the solar wind ram pressure has a role in the Joule heating also during synthetic events that are not as disturbed as the 6 April 2000 event. The influence of the solar wind ram pressure on the Joule heating has to be addressed in future studies. In both simulation cases the amount of Joule heating was smaller as compared to the empirical proxy (Ahn et al., 1983b). In contrast, Lopez et al. (1998) reported an LFM simulation result of a small substorm, in which the Joule heating was large compared to data-based estimation. These discrepancies are due to the different implementation of the simulation codes, however, significant progress in the simulation development could be made by comparing the different codes systematically. Namely, as it is possible that GUMICS-4 gives too low levels of Joule heating whereas LFM seems to give too large values for the Joule heating, the reality may be in between. However, before a systematic comparison between the codes is worthwhile to be carried out, GUMICS-4 results need to be compared with measurement-based estimates of Joule heating. Since there is currently no other measurement-based global estimate of the Joule heating other than

the AMIE technique, comparison to AMIE is the first step.

The current development of the global MHD codes aims to increase the computational capability such that the codes can be run in real time for space weather purposes. However, although GUMICS-4 is only in the process of being parallelized and as such it is still quite slow, a different but possibly as fruitful strategy can be conducted to use GUMICS-4 for space weather purposes. Namely, if the ionospheric dissipation in the simulation corresponds also to actual measurements as it does to the empirical proxies, Eq. (4.7) may have potential in space weather predictions, since one could in principle calculate the ionospheric power consumption from solar wind measurements only. The first results from the two simulated events show that the total ionospheric dissipation in the code can be predicted with over 90% correlation from the solar wind observations. Adding more events, particularly those that are fundamentally different from the two simulated events, to the statistics can give more credibility to Eq. (4.7). However, first the GUMICS-4 ionospheric power output must be calibrated against actual measurements. If this strategy turns out to predict the ionospheric power consumption reliably compared to measurements and also during other events, also other simple power laws for other purposes can in principle be produced. For example, the space weather forecasters do not have a reliable prediction method for the oval location. This could be another relatively simple task where GUMICS-4 could be used in the same manner as it was used in predicting the ionospheric power consumption from the solar wind measurements.

6 Appendix

The following animations are included in the attached CD-rom (in .qt and .avi formats). The animations can be freely used for scientific purposes.

1. Animation on the 6 April 2000 storm simulation, density color-coded, blue lines are the solar wind flow lines and the yellow lines are the magnetic field line (file:aprilstorm.qt).

2. Animation of the simulation environment at the Geotail orbit (shown as white circle) during the 6 April 2000 simulation. X and Y directions are fixed and the Z value indicated at the top of the animation corresponds to the Geotail location (file: geotail_apr_xy.qt).

3. Animation of the simulation environment at the GOES-8 orbit (shown as white circle) during the 6 April 2000 simulation. X and Y directions are fixed and the Z value indicated at the top of the animation corresponds to the GOES-8 location (file: goes8_apr_xy.qt).

4. Animation of the magnetopause surface motion during the 6 April 2000 storm simulation (file: surface_apr.qt).

References

Ahn, B.-H., Robinon, R. M., Kamide, Y., and Akasofu, S.-I., Electric conductivities, electric fields and auroral particle energy injection rate in the auroral ionosphere and their empirical relations to the horizontal magnetic disturbances, *Planet Space Sci., 31*, 641-653, 1983a.

Ahn,B.-H., Akasofu,S.-I., Kamide,Y., The Joule heat production rate and the particle energy injection rate as a function of the geomagnetic indices AE and AL, *J. Geophys. Res., 88*, 6275-6287, 1983b.

Akasofu, S.-I., The development of the auroral substorm, *Planet Space Sci., 12*, 273-301, 1964.

Akasofu, S.-I., Energy coupling between the solar wind and the magnetosphere, *Space Sci. Rev., 28*, 121-190, 1981.

Alfvén, H., On sunspots and the solar cycle, *Ark. f. Mat. Ast. Fys., 29A*, 1-17, 1943.

Axford, W. I., and Hines, C. O., A unifying theory of high-latitude geophysical phenomena and geomagnetic storms, *Can. J. Phys. 39*, 1433-1464, 1961.

Baker, D. N., Pulkkinen, T. I., Angelopoulos, V., Baumjohann, W., and McPherron, R. L., Neutral line model of substorms: Past results and present view, *J. Geophys. Res., 101*, 12,957-13,010, 1996.

Baker, D. N., Pulkkinen, T. I., Hesse, M., and McPherron, R. L., A quantitative assessment of energy storage and release in the Earth's magnetotail, *J. Geophys. Res., 102*, 7159-7168, 1997.

Boteler, D.H., Pirjola, R.J., and Nevanlinna, H., The Effects of Geomagnetic Disturbances on Electrical Systems at the Earth's Surface, *Adv. Space Res., 22*, 17-27, 1998.

Boström, R., Electrodynamics of the ionosphere, in *Cosmical Geophysics*, edited by A. Egeland, Ø. Holter, and A. Omholt, Scandinavian University Books, Copenhagen, Denmark, 1974.

Brackbill, J. U., and Barnes, D. C., The effect of nonzero $\nabla \cdot \mathbf{B}$ on the numerical solutions of the magnetohydrodynamic equations, *J. Comput. Phys., 35*, 426-430, 1980.

Brecht,S.H., Lyon,J.G., Fedder,J.A., Hain,K., A time dependent three-dimensional simulation of the earth's magnetosphere - Reconnection events, *J. Geophys. Res., 87*, 6098-6108, 1982.

Burch, J. L., Rate of erosion of dayside magnetic flux based on a quantitative study of the dependence of polar cusp latitude on the interplanetary magnetic field, *Radio Sci., 8*, 955-961, 1973.

Burton, R. K., McPherron, R. L., and Russell, C. T., An empirical relationship between interplanetary conditions and Dst, *J. Geophys. Res., 80*, 4204-4214, 1975.

Carlowicz, M. J., and Lopez, R. E., Storms from the Sun - the emerging science of space weather, Joseph Henry Press, Washington DC, USA, 2002

Chapman S., Earth storms: Retrospect and prospect, *J. Phys. Soc. Jpn., 17(Suppl. A-1)*, 6-16, 1962.

Chapman S. and Ferraro, V. C. A., A new theory of magnetic storms, 1, The initial phase, *J. Geophys. Res., 36*, 77, 1931a.

Chapman S. and Ferraro, V. C. A., A new theory of magnetic storms, 1, The initial phase (continued), *J. Geophys. Res., 36*, 171, 1931b.

Chapman S. and Bartels, J., Geomagnetism, Oxford University Press, 1940.

Daglis, I. A., The role of magnetosphere-ionosphere coupling in magnetic storm dynamics, in *Magnetic Storms, Geophys. Monogr., 98*, edited by B. T. Tsurutani et al., 107-116, AGU, Washington DC, 1997.

Dessler, A. J., and Parker, E. N., Hydromagnetic theory of magnetic storms, *J. Geophys. Res., 64*, 2239-2259, 1959.

Dungey, J. W., Interplanetary magnetic field and the auroral zones, *Phys. Rev. Lett.,*

6, 47-48, 1961.

Fairfield, D. H., Average and unusual location of the Earth's magnetopause and bow shock, *J. Geophys. Res., 76*, 6700-6716, 1971.

Fedder, J. A., and Lyon, J. G., The Earth's magnetosphere is 165 R_E long: or self-consistent currents, convection, magnetospheric structure and processes for northward interplanetary magnetic field, *J. Geophys. Res., 100*, 3623-3635, 1995.

Fedder,J.A., Lyon,J.G., Slinker,S.P., Mobarry,C.M., Topological structure of the magnetotail as a function of interplanetary magnetic field direction, *J. Geophys. Res., 100*, 3613-3622, 1995a.

Fedder,J.A., Slinker,S.P., Lyon,J.G., Elphinstone, R. D., Global numerical simulation of the growth phase and the expansion onset for a substorm observed by Viking, *J. Geophys. Res., 100*, 19,083-19,093, 1995b.

Fujii, R., Nozawa, S., Buchert, S., and Brekke, A., Statistical characteristics of electromagnetic energy transfer between the magnetosphere, the ionosphere, and the thermosphere, *J. Geophys. Res., 104*, 2357-2365, 1999.

Furth, H. P., Killeen, J., and Rosenbluth, M. N., Finite-resistivity instabilities of a sheet pinch, *Phys. Fluids, 16*, 1054-1063, 1963.

Gonzalez,W.D., and Tsurutani,B.T., Criteria of interplanetary parameters causing intense magnetic storms (Dsr < -100 nT), *Planet Space Sci., 35*, 1101-1109, 1987.

Gonzalez,W.D., Joselyn,J.A., Kamide,Y., Kroehl,H.W., Rostoker,G., Tsurutani,B.T., and Vasyliunas,V.M., What is a geomagnetic storm? *J. Geophys. Res., 99*, 5771-5792, 1994.

Gosling, J. T., McComas, D., J., Phillips, J. L., and Bame, S. J., Geomagnetic activity associated with Earth passage of interplanetary shock disturbances and coronal mass ejections. *J. Geophys. Res., 96*, 7831-7839, 1991.

Greenstadt, E. W., Collisionless shock waves in solar terrestrial environment, in *Solar terrestrial physics: Present and Future*, edited by D. M. Butler and K. Papadopoulos, *NASA Ref. Publ. 1120*, 1984.

Hamilton, D. C., Gloeckler, G., Ipavich, F. M., Studemann, W., Wilken, B., and Kremser, G., Ring current development during the great geomagnetic storm of February 1986, *J. Geophys. Res., 93*, 14,343-14,355, 1988.

Heikkila, W. J., and J. D. Winningham, Penetration of magnetosheath plasma to low altitudes through the dayside magnetospheric cusps, *J. Geophys. Res., 76*, 883-891, 1971.

Ho, C. M., Tsurutani, B. T., Smith, E. J., and Feldman, W. C., A detailed examination of a X-line region in the distant tail: ISEE-3 observations of jet flow and B_z reversals and pair of slow shocks, *Geophys. Res. Lett., 21*, 3031-3034, 1994.

Hones, E. W., Jr., Asbridge, J. R., Bame, S. J., Montgomery, M. D., Singer, S., and Akasofu, S.-I., Measurements of magnetotail plasma flow made with Vela 4B, *J. Geophys. Res., 77*, 5503-5522, 1972.

Ieda, A., Machida, S., Mukai, T., Saito, Y., Yamamoto, T., Nishida, A., Terasawa, T., Kokubun, S., Statistical analysis of the plasmoid evolution with Geotail observations, *J. Geophys. Res., 103*, 4453-4465, 1998.

Janhunen, P., GUMICS-3: A global ionosphere-magnetosphere coupling simulation with high ionospheric resolution, in *Proceedings of Environmental Modelling for Space-Based Applications, Sept. 18-20 1996*, *Eur. Space Agency Spec. Publ., ESA SP-392*, 1996.

Janhunen, P., A positive conservative method for magnetohydrodynamics based on HLL and Roe methods, *J. Comput. Phys., 160*, 649-661, 2000.

Janhunen, P., and Huuskonen, A., A numerical ionosphere-magnetosphere coupling model with variable conductivities, *J. Geophys. Res., 98*, 9519-9530, 1993.

Janhunen, P., and H. E. J. Koskinen, The closure of Region-1 field-aligned current in MHD simulation, *Geophys. Re. Lett., 24*, 1419-1422, 1997

Janhunen, P., and Olsson, A, The current-voltage relationship revisited: exact and approximate formulas with almost general validity for hot magnetospheric electrons for bi-Maxwellian and kappa distributions, *Ann. Geophys., 16*, 292-297, 1998.

Janhunen, P., and Palmroth, M., Some observational phenomena are well reproduced by our global MHD while others are not: Remarks on what, why and how, *Adv. Space Res., 28*, 1685-1691, 2001.

Janhunen, P., Koskinen, H. E. J., and Pulkkinen, T. I., A new global ionosphere-magnetosphere coupling simulation utilizing locally varying time step, in *Proceedings of Third International Conference on Substorms (ICS 3), Versailles, France, May 12-17*, *Eur. Space Agency Spec. Publ., ESA SP-389*, 1996.

Jones, F. C., and Ellison, D. C., The plasma physics of shock acceleration, *Space Sci. Rev., 58*, 259-346, 1991.

Kallio, E. J., and Koskinen, H. E. J., A semiempirical magnetosheath model to analyze the solar wind-magnetosphere interaction, *J. Geophys. Res., 105*, 27,469-27,479, 2000.

Kamide, Y., Is substorm a necessary condition for a magnetic storm, *J. Geomag. Geoelectr., 44*, 109-117, 1992.

Kamide, Y., and Baumjohann, W., Magnetosphere - ionosphere coupling, Springer-Verlag, Berlin, Germany, 1993.

Kamide, Y., Baumjohann, W., Daglis, I. A., Gonzalez, W. D., Grande, M., Joselyn, J. A., McPherron, R. L., Phillips, J. L., Reeves, E. G. D., Rostoker, G., Sharma, A. S., Singer, H. J., Tsurutani, B. T., Vasyliunas, V. M., Current understanding of magnetic storms: Storm-substorm relationships, *J. Geophys. Res., 103*, 17,705-17,728, 1998.

Knipp, D. J., Emery, B. A., Engebretson, M., Li, X., McAllister, A. H., Mukai, T., Kakubun, S., Reeves, G. D., Evans, D., Obara, T., Pi, X., Rosenberg, T., Weatherwax, A., McHarg, M. G., Chun, F., Mosely, K., Codrescu, M., Lanzerotti, L., Rich, F. J., Sharber, J., Wilkinson, P., An overview of the early November 1993 geomagnetic storm, *J. Geophys. Res., 103*, 26,197-26,220, 1998.

Koskinen, H. E. J., and Tanskanen, E., Magnetospheric energy budget and the epsilon parameter, *J. Geophys. Res., 107(A11)*, 1415, doi:10.1029/2002JA009283, 2002.

Kullen, A., and Janhunen, P., MHD simulations of the influence of the IMF clock angle on tail topology and polar cap boundary, submitted manuscript, 2003.

Landau, L. D., and Lifshitz. E. M., Fluid mechanics, Pergamon Press, 1959.

Lemaire, J., Impulsive penetration of filamentary plasma elements into the magnetospheres of the Earth and Jupiter, *Planet Space Sci., 25*, 887-890, 1977.

LeVeque, R. J., Numerical methods for conservation laws, Birkhäuser, 1992.

Lopez, R. E., Goodrich, C. C., Wiltberger, M., and Papdopoulos, K., Simulation of the March 9, 1995 substorm and initial comparison to data, in *Geospace mass and energy flow: Results from the international solar-terrestrial physics program*, Geophysical Monograph 104, American Geophysical Union, Washington DC, USA, pp. 237-245, 1998.

Lu, G., Baker, D. N., McPherron, R. L., Farrugia, C. J., Lummerzheim, D., Ruohoniemi, J. M., Rich, F. J., Evans, D. S., Lepping, R. P., Brittnacher, M., Li, X., Greenwald, R., Sofko, G., Villain, J., Lester, M., Thayer, J., Moretto, T., Milling, D., Troshichev, O., Zaitzev, A., Odintzov, V., Makarov, G., and Hayashi, K., Global energy deposition during the January 1997 magnetic cloud event, *J. Geophys. Res., 103*, 11,685-11,694, 1998.

Luhmann, J. G., Walker, R. J., Russell, C. T., Crooker, N. U., Spreiter, J. R., and Stahara, S. S., Patterns of potential magnetic field merging sites on the dayside magnetopause, *J. Geophys. Res., 89*, 1739-1742, 1984.

Lui, A. T. Y., Current disruption in the Earth's magnetosphere: Observations and models, *J. Geophys. Res., 101*, 13,067-13,088, 1996.

Lyons, L. R., Substorms: Fundamental observational features, distinction from other disturbances, and external triggering, *J. Geophys. Res., 101*, 13,011-13,026, 1996.

Marklund, G. T., Karlsson, T., Blomberg, L. G., Lindqvist, P.-A., Fälthammar, C.-G., Johnson, M. L., Murphree, J. S., Andersson, L., Eliasson, L., Opgenoorth, H. J., and Zanetti, L. J., Observations of the electric field fine structure associated with the westward traveling surge and large-scale auroral spirals, *J. Geophys. Res., 103*, 4125-4144, 1998.

McPherron, R. L., Growth phase of magnetospheric substorms, *J. Geophys. Res., 75*, 5592-5599, 1970.

McPherron, R. L., Magnetospheric substorms, *Rev. Geophys. Space Phys., 17*, 657-681, 1979.

McPherron, R. L., The role of substorms in the generation of magnetic storms, in *Magnetic Storms, Geophys. Monogr., 98*, edited by B. T. Tsurutani et al., 131-147, AGU, Washington DC, 1997.

Meng, C.-I., and Anderson, K. A., A layer of energetic electrons (E>40 keV) near the magnetopause, *J. Geophys. Res., 75*, 1827-1836, 1970.

Mobarry, C., Fedder, J. A., and Lyon, J. G., Equatorial plasma convection from global simulations of the Earth's magnetosphgere, *J. Geophys. Res., 101*, 7859-7874, 1996.

Newell, P. T., and Meng, C.-I., The cusp width and B_z: Observations and a conceptual model, *J. Geophys. Res., 92*, 13,673-13,678, 1987.

Newell, P. T., and Meng, C.-I., The cusp and the cleft/boundary layer: Low-altitude identification and statistical local time variation, *J. Geophys. Res., 93*, 14,549-14,556, 1988.

Newell, P. T., and Meng, C.-I., Ionospheric projections of magnetospheric regions under low and high solar wind pressure conditions, *J. Geophys. Res., 99*, 273-286, 1994.

Newell, P. T., and Sibeck, D. G., B_y fluctuations in the magnetosheath and azimuthal flow velocity transients in the dayside ionosphere, *Geophys. Res. Lett., 20*, 1729-1722, 1993.

Newell, P. T., Meng, C.-I., and Sibeck, D. G., Some low-altitude cusp dependencies on the interplanetary magnetic field *J. Geophys. Res., 94*, 8921-8927, 1989.

Nishida,A., Yamamoto,T., Tsuruda,K., Hayakawa,H., Matsuoka,A., Kokubun,S., Nakamura,M., and Maezawa,K., Structure of the neutral sheet in the distant tail (x = -210 R_E) in geomagnetically quiet times, *Geophys. Res. Lett., 21*, 2951-2954, 1994.

Ogino,T., A three-dimensional MHD simulation of the interaction of the solar wind with

the earth's magnetosphere - The generation of field-aligned currents, *J. Geophys. Res., 91*, 6791-6806, 1986.

Olson, W. P., and Pfitzer, K. A., Magnetospheric response to the gradient drift entry of solar wind plasma, *J. Geophys. Res., 90*, 10,823-10,833, 1985.

Østgaard,N., Stadsnes,J., Bjordal,J., Germany,G.A., Vondrak,R.R., Parks,G.K., Cummer,S.A., Chenette,D.L., Pronko,J.G., Auroral electron distributions derived from combined UV and X-ray emissions, *J. Geophys. Res., 106*, 26,081-26,090, 2001.

Østgaard, N., Vondrak, R. R., Gjerloev, J. W., and Germany, G., A relation between the energy deposition by electron precipitation and geomagnetic indices during substorms, *J. Geophys. Res., 107(A9)*, 1246, doi:10.1029/2001JA002003, 2002.

Palmroth, M., Laakso, H., Fejer, B. G., Pfaff, R. F., Jr., DE 2 observations of morningside and eveningside plasma density depletions in the equatorial ionosphere, *J. Geophys. Res., 105*, 18,429-18,442, 2000.

Palmroth, M., Janhunen, P., and Pulkkinen, T., MHD simulations of dayside magnetospheric boundaries, in *Proc. of ISSS-6*, edited by J. Büchner, C. T. Dum, and M. Scholer, Copernicus Gesellschaft, 114-117, 2001.

Palmroth, M., Pulkkinen, T., and Janhunen, P., MHD simulation of energy transfer from the solar wind into the magnetosphere, in *Proc. of ICS-6*, edited by R. M., Winglee, University of Washington, USA, 205-210, 2002.

Papadopoulos, K., Goodrich, C., WIltberger, M., Lopez, R., and Lyon, J. G., The physics of substorms as revealed by the ISTP, *Phys. Chem. Earth (c), 24*, 189-202, 1999.

Parker, E. N., Sweet's mechanism for merging magnetic fields in conducting fluids, *J. Geophys. Res., 62*, 509-520, 1957.

Petchek, H. E., Magnetic field annihilation, in, *Physics of Solar Flares*, editor W. N. Hess, NASA SP-50, Washington DC, 425-439, 1964.

Powell, K. G., Roe, P. L., Linde, T. J., Gombosi, T. I., and DeZeeuw, D. L., A solution-adaptive upwind scheme for ideal magnetohydrodynamics, *J. Comput. Phys., 154*, 284-309, 1999.

Priest, E., and Forbes, T., Magnetic reconnection: MHD theory and applications, Cambridge University Press, Cambridge, UK, 2000.

Pritchett, P. L., and Coroniti, F. V., Formation of thin current sheets during plasma sheet convection, *J. Geophys. Res., 100*, 23,551-23,566, 1995.

Pulkkinen, T. I., and Wiltberger, M., Thin current sheet evolution as seen in obser-

vations, empirical models, and MHD simulations, *Geophys. Res. Lett., 27*, 1363-1366, 2000.

Pulkkinen, T. I., Baker, D. N., Wiltberger, M., Goodrich, C., Lyon, J. G., and Lopez, R. E., Pseudobreakup and substorm onset: Observations and MHD simulations compared, *J. Geophys. Res., 103*, 14,847-14854, 1998.

Pulkkinen, T. I., Ganushkina, N. Yu., Tanskanen, E. I., Lu, G., Baker, D. N., Turner, N. E., Fritz, T. A., Fennel, J. F., and Roeder, J., Energy dissipation during a geomagnetic storm: May 1998, *Adv. Space Res., 30*, 2231-2240, 2002.

Raeder, J., Walker, R. J., and Ashour-Abdalla, M., The structure of the distant tail during long periods of northward IMF, *Geophys. Res. Lett., 22*, 349-352, 1995.

Raeder, J., Berchem, J., and Ashour-Abdalla, M., The Geospace Environment Modeling grand challenge: Results from a Global Geospace Circulation Model, *J. Geophys. Res., 103*, 14,787-14,797, 1998.

Reiff, P. H., Spiro, R. W., and Hill, T. W., Dependence of polar cap potential on interplanetary parameters, *J. Geophys. Res., 86*, 7639-7648, 1981.

Richmond,A.D., and Kamide,Y., Mapping electrodynamic features of the high-latitude ionosphere from localized observations - Technique, *J. Geophys. Res., 93*, 5741-5759, 1988.

Robinson, R. M., Vondrak, R. R., Miller, K., Dabbs, T., and Hardy, D., On calculating ionospheric conductances from he flux and energy of precipitating electrons, *J. Geophys. Res., 92*, 2565-2569, 1987.

Rosenbauer, H., Gruenwaldt, H., Montgomery, M. D., Paschmann, G., and Skopke, N., HEOS 2 plasma observations in the distant polar magnetosphere: The plasma mantle, *J. Geophys. Res., 80*, 2723-2737, 1975.

Sckopke, N., A general relation between the energy of trapped particles and the disturbance field near the Earth, *J. Geophys. Res., 71*, 3125-3130, 1966.

Scurry, L., and Russell, C. T., Proxy studies of energy trasnfer to the magnetosphere, *J. Geophys. Res., 96*, 9541-9548, 1991.

Shue,J.-H., Song,P., Russell,C.T., Steinberg,J.T., Chao,J.K., Zastenker,G., Vaisberg,O.L., Kokubun,S., Singer,H.J., Detman,T.R., Kawano,H., Magnetopause location under extreme solar wind conditions, *J. Geophys. Res., 103*, 17,691-17,700, 1998.

Sibeck, D. G., and Gosling, J. T., Magnetosheath fluctuations and magnetopause motion, *J. Geophys. Res., 101*, 31-40, 1996.

Sibeck, D. G., Paschmann, G., Treumann, R. A., Fuselier, S. A., Lennartsson, W., Lock-

wood, M., Lundin, R., Ogilvie, K., W., Onsager, T., G., Phan, T.-D., Roth, M., Scholer, M., Sckopke, N., Stasiewicz, K., and Yamauchi, M., Plasma transfer processes at the magnetopause, in *Magnetospheric Plama sources and losses*, edited by B. Hultqvist, M. Øieroset, G. Paschmann, and R. Treumann, Kuwer Academic Publishers, the Netherlands, pp. 207-285, 1999

Singer, S. F., A new model of magnetic storms and aurorae, *EOS Trans., AGU, 38*, 175, 1957.

Siscoe, G. L., Crooker, N. U., and Siebert, K. D., Transpolar potential saturation: Roles of Region 1 current system and solar wind ram pressure, *J. Geophys. Res., 107(A10)*, 1321, doi:10.1029/2001JA009176, 2002.

Slinker, S. P., Fedder, J. A., Emery, B. A., Baker, K. B., Lummerzheim, D., Lyon, J. G., and Rich, F. J., Comparison of global MHD simulations with AMIE simulations for the events of May 19-20, 1996, *J. Geophys. Res., 104*, 28,379-28,395, 1999.

Smith, M. F., and Lockwood, M., Earth's magnetospheric cusps, *Rev. Geophys., 34*, 233-260, 1996.

Spiro, R. W., Reiff, D. H., and Mather, L. J., Jr., Precipitating electron average flux and auroral zone conductances - An empirical model, *J. Geophys. Res., 87*, 8215-8227, 1982.

Stasiewicz, K., Finite Larmor radius effect in the magnetosphere, *Space Sci. Rev., 65*, 221-252, 1994.

Sweet, P. A., The neutral point theory of solar flares, in *Electromagnetic Phenomena in Cosmical Physics* IAU Symp. 6, ed. B. Lehnert, Cambridge University Press, 123-134, 1958.

Tanaka, T., Finite volume TVD scheme on an unstructured grid system for three-dimensional MHD simulation of inhomogenous systems including strong background potential fields, *J. Comput. Phys., 111*, 381-389, 1994.

Tanskanen, E. I., Pulkkinen, T. I., Koskinen, H. E. J., and Slavin, J. A., Substorm energy budget near solar minimum and maximum: 1997 and 1999 compared, *J. Geophys. Res., 107*, 10.1029/2001JA900153, 2002.

Topliss, S., Owen, C. J., and Peterson, W. K., A simple model of complex cusp ion dispersions during intervals of northward interplanetary magnetic field, *Geophys. Res. Lett., 27*, 3587-3590, 2000.

Tsurutani,B.T. and Thorne,R.M., Diffusion processes in the magnetopause boundary layer, *Geophys. Res. Lett., 9*, 1247-1250, 1982.

Tsyganenko, N. A., and Russell, C. T., Magnetic signatures of the distant polar cusps:

Observations by Polar and quantitative modeling, *J. Geophys. Res., 104*, 24,939-24,955, 1999.

Turner, N. E., Baker, D. N., Pulkkinen, T. I., Roeder, J. L., Fennell, J. F., and Jordanova, V. K., Energy content in the storm time ring current, *J. Geophys. Res., 106*, 19,149-19,156, 2001.

Walker, R. J., Ogino, T., Raeder, J., and Ashour-Abdalla, M., A global magnetohydrodynamic simulation of the magnetosphere when the interplanetary mahnetic field is southward: The onset of magnetotail reconnection, *J. Geophys. Res., 98*, 17,235-17,249, 1993.

Zhou, X. W., Russell, C. T., Le, G., Fuselier, S. A., and Scudder, J. D., Solar wind control of the polar cusp at high altitude, *J. Geophys. Res., 105*, 245-251, 2000.